

FURTHER DEVELOPMENTS AND APPLICATION OF THE METHOD OF  
SELECTIVE PHYSISORPTION  
FOR MEASURING ACTIVE CATALYST SURFACE AREA

By

Irfan Ali Toor

A DISSERTATION PRESENTED TO THE GRADUATE  
SCHOOL OF THE UNIVERSITY OF FLORIDA IN PARTIAL  
FULFILLMENT OF THE REQUIREMENTS FOR THE  
DEGREE OF DOCTOR OF PHILOSOPHY

UNIVERSITY OF FLORIDA

1985

## ACKNOWLEDGMENTS

The author wishes to express his profound gratitude towards Dr. Hong H. Lee, chairman of the advisory committee, for suggesting this project and for his patience and continued guidance throughout this work.

The author also wishes to acknowledge his gratitude towards Dr. Gar B. Hoflund, Dr. J.P. O'Connell, Dr. G.B. Westerman-Clark and Dr. E.R. Allen for serving on the advisory committee and for their valuable criticism of the manuscript. Sincere appreciation is also extended to Mr. Tracy Lambert, Mr. Ron Baxley and Mr. Rudi Strohschein for their skilled services in fabricating the experimental apparatus.

Finally, the author wishes to thank his parents, brothers, sisters, wife and child for their patience and invaluable moral support without which the completion of this work would not have been possible.

## TABLE OF CONTENTS

	Page
ACKNOWLEDGMENTS.....	i i
KEY TO SYMBOLS.....	v
ABSTRACT.....	v i
 CHAPTERS	
I INTRODUCTION.....	1
II MODIFICATIONS AND IMPROVEMENTS IN THE METHOD OF SELECTIVE PHYSISORPTION.....	7
Experimental Modifications.....	8
Theoretical Modifications.....	8
III APPLICATION OF THE SELECTIVE PHYSISORP- TION METHOD TO METAL CATALYST.....	15
Experimental Apparatus And Procedure.....	16
Catalyst Preparation.....	18
Results And Discussion.....	19
IV APPLICATION OF THE METHOD OF SELECTIVE PHYSISORPTION TO OXIDE CATALYST.....	31
Experimental Apparatus.....	32
Experimental Procedure.....	38
Catalyst Preparation.....	40
Experimental Results And Discussion.....	41
Summary.....	68
V CONCLUSIONS AND RECOMMENDATIONS.....	73
 APPENDICES	
A PREPARATION OF OXIDE CATALYSTS.....	80

B	NITROUS OXIDE SELECTIVE PHYSISORPTION DATA FOR PLATINUM SILICA CATALYST.....	82
C	NITROUS OXIDE SELECTIVE PHYSISORPTION DATA FOR THE OXIDE CATALYSTS.....	86
D	NITROGEN PHYSISORPTION RAW DATA.....	90
E	DIFFERENTIAL REACTOR DATA.....	110
F	ERROR ANALYSIS OF THE PACKING FACTOR VALUES....	113
	LIST OF REFERENCES.....	114
	BIOGRAPHICAL SKETCH.....	116

## KEY TO SYMBOLS

$b_i$	proportionality constant in Eq. (10)
$I_1$	integral defined by Eq. (7) or by Eq. (8)
$I_t$	integral defined by Eq. (8) or by Eq. (12)
$R_1$	volume of gas adsorbed on catalyst per unit surface area of the catalyst in the supported state
$R_2$	volume of gas adsorbed on support per unit area of the support in the supported state
$S_1$	catalyst surface area
$S_2$	support surface area
$S_t$	total surface area ( $S_1+S_2$ )
$T$	temperature
$T_i$	lower limit for integration with respect to temperature
$T_f$	upper limit for integration with respect to temperature
$U_i$	volume of gas adsorbed on pure catalyst ( $i=1$ ) or pure support ( $i=2$ )
$v_1$	volume of gas adsorbed on the catalyst in the supported state
$v_2$	volume of gas adsorbed on the support in the supported state
$v_t$	$v_1+v_2$
$\gamma_1$	$U_1/S_1$
$\gamma_2$	$U_2/S_2$
$\gamma_t$	$v_t/S_t$
Subscript $i = 1$ for catalyst, $2$ for support	

Abstract of Dissertation Presented to the Graduate School  
of the University of Florida in Partial Fulfillment of the  
Requirements for the Degree of Doctor of Philosophy

FURTHER DEVELOPMENTS AND APPLICATION OF THE METHOD OF  
SELECTIVE PHYSISORPTION  
FOR MEASURING ACTIVE CATALYST SURFACE AREA

By

Irfan Ali Toor

May, 1985

Chairman: Dr. H.H. Lee

Major Department: Chemical Engineering

Modifications have been made in the method of selective physisorption as developed by Miller and Lee (Miller, D.J., and H.H. Lee, AIChE J., 30, 84 (1984)). The new method makes use of packing factors of the selectively physisorbed gas instead of fractional coverage. The spread of packing factors versus temperature curves has been shown to be much greater than the spread of fractional coverage versus temperature curves. The method has been tested on a standard catalyst system of platinum supported on silica. The results have been compared with the results of hydrogen chemisorption and it has been observed that they are in fair agreement. The application of the new method has been extended to metal oxide catalysts. The results indicate that nitrous oxide is not the best suited adsorbate for the moly-alumina catalyst, in the

sense that the nitrous oxide selective physisorption does not yield the absolute value of the fractional surface area of this catalyst. However, it can still be used to determine the ratios of the fractional surface areas of different moly-alumina catalysts with up to 15 wt%MoO<sub>3</sub> loading. The values of the fractional surface area ratios calculated from the nitrous oxide selective physisorption results were much lower than the values computed from the BET results, assuming an epitaxial monolayer of moly oxide on the surface of alumina. It was shown that the cyclohexane dehydrogenation activity increases with the increase in nitrous oxide packing factors for the moly-alumina catalysts. The nitrous oxide selective physisorption was not successful on moly-silica catalyst.

## CHAPTER 1 INTRODUCTION

Catalytic materials are prepared with the intention of maximizing the exposed surface area of the active material upon which the reaction may take place. Many important industrial catalysts are prepared by dispersing the active material on the surface of a porous material generally referred to as the support. Since the number of the catalytically active sites is believed to be proportional to the total surface area of the dispersed material it is desirable to measure the surface area of the dispersed catalyst. Unfortunately, direct measurement of the surface area of the catalyst material dispersed in the pores of the support is not possible at the present time. Therefore various indirect techniques have been developed to characterize the dispersed catalyst. X-ray line broadening (Anderson , 1968), mossbauer spectroscopy (Bartholomew and Boudart, 1973), magnetization techniques (Hill and Selwood, 1949), and low angle scattering (Sinfelt, 1967), to mention just a few. Another important method of characterizing the porous catalysts is the physical and chemical adsorption of different gases to determine the surface area of the dispersed catalyst. Brunauer, Emmett, and Teller (1938) were the first to use the low temperature physical adsorption isotherms of



various gases to measure the total surface area of the porous catalysts. This method, commonly known as the BET method, has found wide application in catalytic research all around the world. Brunauer and Emmett (1938, 1940) also studied the selective chemisorption of various gases to determine the surface area of dispersed catalysts. Since that time, numerous attempts have been made to use the method of selective chemisorption to determine the fractional surface area of oxide catalysts but they have met with limited success.

The chemisorption method differs from the physisorption method in that, ideally, the chemical adsorption occurs only onto a particular component of the catalytic material. The method requires that the adsorbate form a monolayer of the chemisorbed atoms on the surface of the catalyst and that there exist a simple relationship between the number of molecules or atoms adsorbed and the number of surface atoms of the catalyst. Since most metals chemisorb small molecules like  $H_2$ ,  $O_2$ , and CO the chemisorption has been quite successful in characterizing many metal catalysts. For instance hydrogen chemisorption has been used very effectively to determine the fractional surface area of dispersed platinum catalysts (Spenedal and Boudart, 1960; Adler and Kearney, 1960). In the case of the metal oxide catalysts, however, the situation is further complicated because of two problematic points : (a) the lower interaction specificity of the possible gas/metal oxide system relative to that for

gas/support system, and (b) the necessity to look for different gases for each supported metal oxide catalyst. Nevertheless, numerous attempts have been made to use selective chemisorption of gases to characterize metal compound and metal oxide catalysts (Weller and Voltz, 1954 ; Segawa and Hall, 1983) but difficulty in the interpretation of the experimental results still remains. A series of articles has been published by Weller and associates (Parekh and Weller, 1977; Parekh and Weller, 1978; Srinivasan, Liu, and Weller, 1979; Liu, Yuan, and Weller, 1980; Garcia Fierro, Mendioroz, Pajares, and Weller, 1980; Liu and Weller, 1980) to discuss the low temperature oxygen chemisorption for measuring the fractional surface area of molybdenum oxide dispersed on alumina but their results are at variance with current ideas concerning the formation of an epitaxial monolayer of molybdenum oxide on the surface of alumina. It has also been shown that in oxide catalysts the chemisorption is site selective (Millman, Crespin, Crillo, Abdo and Hall, 1979; Vaylon and Hall, 1983) and therefore represents only a fraction of the actual surface area of the dispersed catalyst. From the above discussion it is clear that there was a need to look into new methods of gas adsorption of porous catalysts which may be applicable to a wider range of catalysts including metal and metal oxide catalysts.

A new experimental method of measuring the active surface area of supported catalysts using selective physisorption of certain gasses has been put forward recently by

Miller and Lee (1984). The basic idea here was that a mono- or sub-monolayer volume of a gas physisorbed on a two component solid as in a supported catalyst should be able to distinguish between the two different surfaces upon thermal desorption if the interactions between the gas and the surface are strong, say 3-6 Kcal/mole in terms of heats of adsorption. The desorption characteristics of gas coverage with temperature for the catalyst, the support, and the supported catalyst were used by Miller and Lee (1984) to calculate the fraction of the total surface area occupied by the catalyst. Because of the nature of physisorption the selective physisorption should be applicable to any supported catalyst including oxides and metal compound catalysts provided a suitable adsorbate is used. This is in contrast to the chemisorption method (Spenedal and Boudart, 1960; Adler and Kearney, 1960) which does not yield the catalyst surface area of some metal catalysts and the majority of metal compound catalysts because of the specific nature of chemisorption, although it yields valuable information of the sites active to a chemisorbing gas.

In the original development (Miller and Lee, 1984), thermal desorption of selectively physisorbed carbon dioxide on the surface of potassium carbonate carbonate-carbon black mixtures was used to determine the fractional surface area of each component in the physical mixture. A qualitative comparison between the selective physisorption method and oxygen chemisorption was also given for supported silver

catalyst. Nevertheless, no conclusive evidence was presented as to the effectiveness of the selective physisorption method as applied to the supported catalysts. Further the thermal desorption experiments and the data analysis were such that the method was effective only when catalyst loadings were high and the catalyst covered a significant portion of the total surface area of the support. In Chapter 2, we present refinements in the original method that would allow a more accurate determination of the catalyst surface area even when the catalyst covers a small portion of the support surface area. The new method involves the use of packing factors ( $\gamma$ ) in place of fractional gas coverage ( $\theta$ ) to calculate the fractional surface area of the dispersed catalyst.

The effectiveness of the selective physisorption method in measuring fractional catalyst surface area of dispersed catalyst is demonstrated in the Chapter 3. A catalyst system was sought that is amenable to a well established method of measuring the fractional surface area of the dispersed catalyst. Platinum dispersed on silica was chosen because hydrogen chemisorption has been well established as a reliable method measuring the surface area of dispersed platinum and thus a valuable comparison of results could be made with the results of selective physisorption.

Since an important advantage of the method of selective physisorption would be a more general and wider application to different types of catalysts, it was decided to test the

new method on at least one industrially important metal oxide catalyst. The application of the selective physisorption method to moly-alumina catalyst is presented in Chapter 4. The results are correlated with cyclohexane dehydrogenation activity of the catalyst measured in a differential reactor. Conclusions and recommendations for future work are discussed in the Chapter 5.

## CHAPTER 2 MODIFICATIONS AND IMPROVEMENTS IN THE METHOD OF SELECTIVE PHYSISORPTION

Selective physisorption utilizes the differences in the forces of interaction between different gas solid pairs. A detailed discussion of the nature of the physisorption forces and the kinetic models used to describe this phenomenon has been given by Miller (1982) and will not be presented here. Anyone interested in a more thorough understanding of the subject is referred to Brunauer (1943), Young and Crowell (1962), Clark (1970), Ricca (1972), Herz et al. (1982). The purpose of this research is to advance the theory of selective physisorption as applied to the measurement of the fractional surface area of supported catalyst. A few modifications have been made in the experimental method and the method of data analysis which render the methods of selective physisorption more sensitive to changes in the fractional surface area of the dispersed catalyst. These modifications and improvements will be discussed in the following paragraphs. The main contribution of this study, however, is the demonstration of the effectiveness of the selective physisorption in determining the fractional surface area of supported metal catalysts (Chapter 3), and its extension to oxide catalysts (Chapter 4).

### Experimental Modifications

In the original development, Miller and Lee (1984) utilized the differences in the gas coverage ( $\theta$ ) versus temperature (T) relationships of the mono- or sub-monolayer volume of a physisorbed gas to determine the fraction of the total surface area covered by the catalyst. In order to generate the thermal desorption isobars it was assumed that a pseudo steady state exists during the transient thermal desorption of the mono- or sub-monolayer of the physisorbed gas. Therefore a single thermal desorption was sufficient to obtain a  $\theta$ -T relationship (Miller and Lee, 1984). The pseudo steady state assumption was avoided in this study and instead more than one constant temperature cold baths were used to determine the amount of gas adsorbed at each temperature in order to generate a more accurate  $\theta$ -T relationship. The motivation is that the total desorption will provide a more accurate determination of the amount of gas adsorbed and thus a more accurate adsorption isobar will be achieved which in turn will enhance the accuracy with which the catalyst surface area is determined.

### Theoretical Modifications

While Miller and Lee (1984) have used the  $\theta$ -T relationship to determine the fractional surface area of the supported catalyst, it was found that the use of packing factor (which is the amount of gas adsorbed per unit surface area of the supported catalyst) in place of  $\theta$  would allow a more accurate determination of the fractional surface area of the

supported catalyst. For instance, consider Figure 1, which compares the  $\theta$ -T curves of the pure components of potassium carbonate and carbon black mixture, obtained by Miller and Lee (1984), with the spread of the  $\gamma$  (the packing factor expressed as volume of gas per unit  $N_2$  BET area) versus T curves generated from the same data. It is clear that the spread of the  $\gamma$ -T curves is much greater than the spread of the  $\theta$ -T curves and therefore the former relationship will provide a better sensitivity towards the determination of the fractional surface area of the dispersed catalyst. In light of the above development it was necessary to develop an expression for the determination of the fractional surface based on the packing factors rather than  $\theta$  in order to take advantage of the greater sensitivity afforded by the packing factor.

If we let  $v_1$  and  $v_2$  be the volumes of the submonolayer of a gas adsorbed on the surfaces 1 (catalyst) and 2 (support) in the supported catalyst then the total volume of the gas adsorbed on the supported catalyst  $v_t$  is simply the sum of  $v_1$  and  $v_2$ :

$$v_t(T) = v_1(T) + v_2(T). \quad (1)$$

Further if we let  $x_i(T)$  be the fraction of the surface area of the surface  $i$  that is covered by the adsorbate at the temperature  $T$ , the total surface area of the supported catalyst,  $S_t$ , is given by



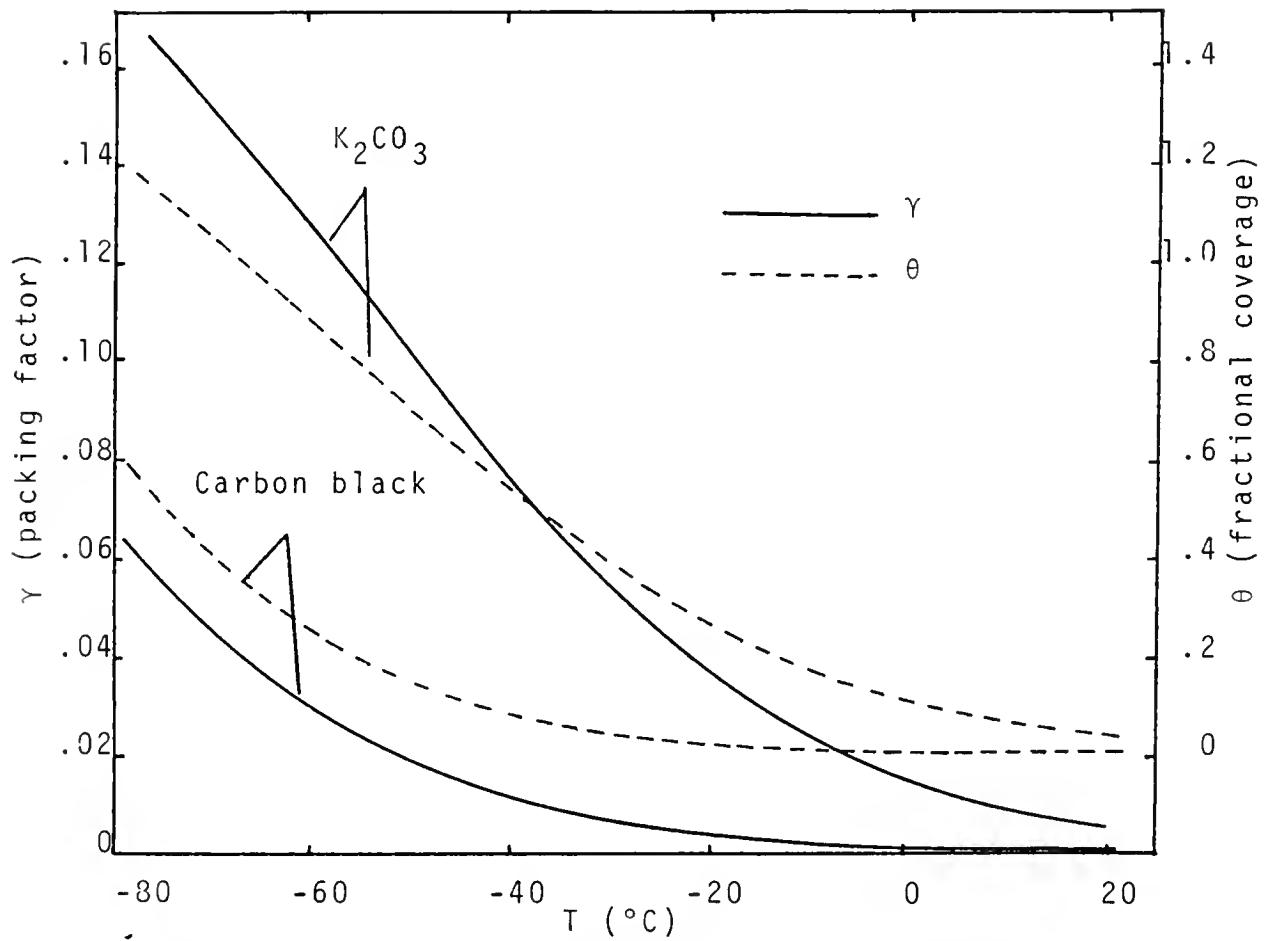


Figure 1. Comparison between  $\gamma$ - $T$  curves and  $\theta$ - $T$  curves for the potassium carbonate-carbon black system.

$$S_t = \frac{v_1}{x_1} \frac{1}{R_1} + \frac{v_2}{x_2} \frac{1}{R_2} \quad (2)$$

where the factor  $R_i$  is given by

$$R_i = \frac{\text{cm}^3 \text{ adsorbate on surface } i}{\text{m}^2 \text{ surface area of surface } i}. \quad (3)$$

Since  $v_i$  cannot be measured directly, but  $v_t$  can be measured using thermal desorption, we rearrange Eq. (2) with the help of Eq. (1) to get

$$v_1(T) = \frac{S_t - \frac{v_t(T)}{R_2 x_2}}{\frac{1}{R_1 x_1} - \frac{1}{R_2 x_2}}. \quad (4)$$

Further the fractional surface area of the dispersed catalyst,  $S_1 / S_t$ , is given by

$$\frac{S_1}{S_t} = \frac{1 - \left[ \frac{v_t(T)}{S_t} \right] \left[ \frac{1}{R_2 x_2(T)} \right]}{1 - \left[ \frac{R_1 x_1(T)}{R_2 x_2(T)} \right]} \quad (5)$$

which follows from Eq. (4) and the relationship

$S_1 = v_1(T) / R_1 x_1(T)$ . It is important to note that the relationship of Eq. (5) yields a value of the fractional surface area of the dispersed catalyst at every temperature at which physisorption can be obtained. Therefore Eq. (5) can be

integrated over the entire temperature range of interest and the result will still be valid. This is done in order to take advantage of the entire adsorption isobar. Also the integration cancels out the scatter in the experimental data and the calculated value will be the average value of the fractional surface area of the dispersed catalyst, representing the temperature range of interest of the adsorption isobar. Multiplying  $S_1 / S_t$  by the numerator of Eq. (5), integrating, and rearranging yield the following final result

$$\frac{S_1}{S_t} = \frac{I_1}{I_t} \quad (6)$$

where

$$I_1 = \int_{T_i}^{T_f} \left[ 1 - \frac{v_t}{S_t} \frac{1}{R_2 x_2} \right] dT \quad (7)$$

and

$$I_t = \int_{T_i}^{T_f} \left[ 1 - \frac{R_1 x_1}{R_2 x_2} \right] dT. \quad (8)$$

Here  $T_i$  and  $T_f$  are the temperatures chosen for integration in the temperature range of interest.

The values of  $R_i x_i$  can readily be obtained experimentally for the two pure components constituting the supported

catalyst. The definitions of  $R_i$  and  $x_i$ , when applied to the pure components, yield

$$[R_i x_i(T)]_{\text{pure}} = \frac{U_i}{(N_2 \text{ BET area})_{i,\text{pure}}} = \gamma_i(T) \quad (9)$$

where  $U_i$  is the sub-monolayer volume of the gas adsorbed on pure catalyst ( $i=1$ ) and pure support ( $i=2$ ) surfaces at temperature  $T$ . It should be noted that  $U_i$  is different from  $v_i$ . For the platinum catalyst supported on silica (Chapter 3), for instance, the volume of gas adsorbed on the platinum particles is  $U_i$  whereas the volume of gas adsorbed on the platinum particles dispersed in the supported catalyst is  $v_1$ . If we assume that the quantity  $R_i x_i$  for the surface unsupported state is proportional to that for the surfaces in the pure state, we have

$$R_i x_i(T) = b_i \gamma_i(T) \quad (10)$$

where  $b_i$  is the proportionality constant. However, if the adsorbate is indeed physisorbed it will not distinguish between pure and dispersed states of the catalyst and therefore the constants  $b_i$  should assume a value of unity. For such an adsorbate,  $R_i x_i$  is equal to  $\gamma_i$  and all the quantities in Eqs. (7) and (8) can readily be obtained from experiments, thus allowing the calculation of the fractional

catalyst surface area from Eq. (6) because Eqs. (7) and (8) reduce to

$$I_1 = \int_{T_i}^{T_f} \left( 1 - \frac{\gamma_t}{\gamma_2} \right) dT \quad (11)$$

$$I_t = \int_{T_i}^{T_f} \left( 1 - \frac{\gamma_1}{\gamma_2} \right) dT \quad (12)$$

where  $\gamma_t = v_t / S_t$ .

### CHAPTER 3

#### APPLICATION OF THE SELECTIVE PHYSISORPTION METHOD TO METAL CATALYSTS

One shortcoming of the work of Miller and Lee (1984) was that no conclusive evidence was provided as to the effectiveness of the selective physisorption method as applied to the dispersed catalysts. They used the selective physisorption of carbon dioxide at  $-78^{\circ}\text{C}$  to determine the fractional catalyst surface area of silver catalyst dispersed on alumina and compared the results with those of oxygen chemisorption. However, the stoichiometry of oxygen chemisorption on dispersed silver catalyst is not fully understood (Miller, 1982) and is not a well established method of measuring the fractional surface area of silver catalyst. Furthermore the comparison made by the original authors was only qualitative in nature, and therefore does not furnish a positive verification of the surface area calculated using thermal desorption of the selectively physisorbed carbon dioxide. Scanning electron microscopy was also attempted to determine the surface area of dispersed silver but the results were inconclusive.

The other catalyst system studied by Miller and Lee (1984) was potassium carbonate dispersed on carbon black. Again no independent measurement of potassium carbonate surface area could be made and thus no comparison was made.

Physical mixtures of carbon black and potassium carbonate were then used to partially verify the results but such a comparison can only be of a limited value.

In order to provide a positive evidence that the selective physisorption method can be used effectively to determine the fractional surface area of dispersed metal catalyst, a catalyst system was sought that would provide an already established alternate method of independently measuring the fractional surface area of the catalyst so that the results of the selective physisorption method could be verified. Platinum supported on silica was chosen because it meets these conditions perfectly. Hydrogen chemisorption has been studied extensively (Spenedal and Boudart, 1960; Adler and Kearney, 1960; Wanke, Lotochinski and Sidwell, 1981; Sarakany and Gonzalez, 1982) and is a well established method of measuring the fractional surface area of platinum catalyst. Therefore it was decided to determine the fractional surface area of platinum in platinum-silica catalyst using the new method and to verify the results by making a comparison with the platinum surface area determined from hydrogen chemisorption. In this manner, it would be possible to demonstrate the effectiveness of the selective physisorption method in determining the fractional surface area of metal catalysts.

#### Experimental Apparatus And Procedure

The gas adsorption experiments in this study have been carried out with the help of a Perkin Elmer continuous flow

sorptometer modified for thermal desorption experiments. A detailed description of this apparatus has been given by Miller (1982) and will not be presented here.

The constant temperature cold baths that were used for low temperature adsorption were made from liquid nitrogen, acetone-dry ice, chloroform-dry ice, and chlorobenzene-dry ice mixtures to obtain  $-196^{\circ}\text{C}$ ,  $-78^{\circ}\text{C}$ ,  $-61^{\circ}\text{C}$ , and  $-45^{\circ}\text{C}$  (Phipps and Hume, 1968) respectively. The sample cell containing the catalyst sample (Miller, 1982) was immersed in the cold bath and the system was allowed to equilibrate. Equilibrium was determined by a constant reading of the temperature recorder for a period of 4-5 minutes, and a stable response from the thermal conductivity cell detector. After the equilibrium had been reached the cold bath was removed instantaneously and the sample was heated with the help of an external heating coil, to completely desorb the gas. The response of the thermal conductivity cell was recorded using an integrator recorder. A minimum of two readings were taken at each adsorption temperature. A 0.5 ml pulse of the adsorbate gas was used to calibrate the response of the thermal conductivity cell.

All samples were processed one after the other within a period of 24 hrs. to ensure minimal fluctuations in the gas flow rate. The gas flow rates were measured with a soap bubble meter after the last sample had been processed, as detailed in the reference.



The hydrogen chemisorption experiments were carried out using the dynamic pulse method (Wanke, Lotochinski and Sidwell, 1981). A detailed description of the method and the experimental apparatus is available in the reference and need not be presented here. Pulses of 0.1 ml of hydrogen (Airco Grade 5.5, 99.9995%) were used for the chemisorption at 100 °C. Each gas was purified by first passing through a bed of 4 Å molecular sieve (Davison Chemical, Grade 5.3, 4-8 mesh beads) and then through a bed of copper.

In the BET and the low temperature adsorption experiments, helium (Airco Grade 4.5, 99.995%) was used as the carrier gas with nitrogen (Linde, Ultra High Purity, 99.999%), carbon dioxide (Airco Grade 4, 99.99%) or nitrous oxide (Matheson, Ultra High Purity, 99.999%) as the adsorbate. Each gas was purified by first passing through a 4 Å molecular sieve (Davison Chemical Grade 5.3, 4-8 mesh beads) which was followed by a cold trap. The cold trap consisted of liquid nitrogen in a dewer flask when nitrogen was used as adsorbate, or acetone-dry ice slush in a dewer flask when nitrous oxide or carbon dioxide was used as the adsorbate.

#### Catalyst Preparation

Platinum-silica catalysts were prepared by impregnating powdered silica (Alpha, 99.5% SiO<sub>2</sub>, -400 mesh amorphous) with chloroplatinic acid solution. A stock solution of chloroplatinic acid was prepared by dissolving 5.1 gm of chloroplatinic acid (Alpha) in 100 ml of distilled water. Impregnation was carried out by adding 11.5, 24.5 ml, and

36.0 ml of the stock solution to three 5 gm samples of sintered silica to prepare 5 wt%, 10 wt%, and 15 wt%Pt catalysts respectively. Each sample was allowed to stand for a 24-hr period for impregnation. Intermittent stirring was continued during this 24-hr period. The samples were then dried in an oven at 120 °C for 24 hrs, and then reduced in flowing hydrogen at 500 °C for 17 hrs.

Another catalyst sample with 1 wt%Pt loading was prepared in the following manner. A calculated amount of chloroplatinic acid which gives 1 wt%Pt loading on 10 grams of silica was dissolved in 5 grams of distilled water. The resulting solution was added to 10 grams of amorphous silica (Alpha, 99.5%SiO<sub>2</sub>, -400 mesh amorphous) to obtain a thick slurry. This was allowed to stand for a 24-hr period for impregnation. During this time, intermittent stirring was continued to maintain a uniform slurry. At the end of the 24-hr period, the impregnated slurry was dried at 120 °C for another 24 hrs. This process was followed by 16 hrs of reduction at 500 °C in a stream of flowing hydrogen. No pre-treatment was carried out to increase the dispersion of any catalyst.

### Results And Discussion

The BET and hydrogen chemisorption results are summarized in Table 1. The BET total surface area for each sample was determined using four data points at four different pressures. A one-to-one hydrogen-to-platinum correspondence was used to convert the amount of hydrogen chemisorbed on

Table 1. BET and H<sub>2</sub> chemisorption results.

Sample	N <sub>2</sub> monolayer volume at STP (ml/gcat)	BET Area (m <sup>2</sup> /gcat)	Amount of H <sub>2</sub> chemisorbed <sup>3</sup> (ml H <sub>2</sub> /gcat *10 <sup>3</sup> )	Active area <sup>*</sup> (m <sup>2</sup> Pt/gcat)
Pt particles	0.16	0.70	- -	- -
SiO <sub>2</sub>	1.53	6.66	- -	- -
1 wt% Pt on SiO <sub>2</sub>	1.22	5.79	67.6	0.324
5 wt% Pt	1.19	5.66	7.7	0.037
10 wt% Pt	1.11	5.26	59.0	0.283
15 wt% Pt	0.96	4.57	54.7	0.262

\*Area calculated from the amount of hydrogen chemisorbed.

the active platinum surface area of the supported catalyst, using a value of  $1.12 \times 10^{19}$  Pt sites/m<sup>2</sup> (Spenedal and Boudart, 1960). It is interesting to note in Table 1 that the total BET surface per gram of supported catalyst decreases with increasing platinum loading. This behavior could be due to a growing number of platinum crystallites as the platinum loading is increased. The large crystallites may block micropores and thereby cause a reduction in the total surface area of the supported catalyst.

The chemisorption results reported in Table 1 (equivalently in Table 2) need some comments. As indicated earlier, the impregnation technique for the 1 wt%Pt catalyst was different from those for 5, 10, 15 wt%Pt samples. As apparent from the table, inefficient impregnation for the higher loading catalysts resulted in low platinum dispersion. Because of the unusual behavior, the chemisorption experiments were repeated only to confirm the reported values in Table 2. This apparent drawback, however, was instrumental in demonstrating that selective physisorption can distinguish small differences in fairly small surface areas, which is an important feature because the technique was shown earlier (Miller and Lee, 1984) to be effective only for large surface areas. One can see for the higher loading sample catalysts that the catalyst surface area increases as the loading increases from 5 to 10 wt%Pt. As the loading is further increased to 15 wt%Pt, the platinum surface area remains essentially the same ( $.28 \text{ m}^2$  versus

0.26 m<sup>2</sup>). This is not very surprising at the high loading with inefficient impregnation. As the chemisorption results for the 1 wt%Pt sample, which was prepared differently, indicates, the impregnation procedures for the sample led to a more efficient dispersion.

The equilibrium adsorption isobars obtained from experiments were normalized with respect to the total BET surface area and the results are shown in Figure 2 for the adsorbate nitrous oxide and in Figure 3 for the adsorbate carbon dioxide. Given on the ordinate are  $\gamma_i(T)$  for the pure platinum and silica and  $v_t / S_t$  for the supported catalyst samples. The fractional catalyst surface area,  $S_1 / S_t$ , can readily be calculated from  $\gamma_i$  and  $v_t / S_t$  given in the Figures 2 and 3 using Eqs. (6) and (10), provided  $b_i$  are known.

As indicated earlier, the values of  $b_i$  should be unity if the adsorbate is indeed physisorbed. For the results given in Figure 2, which is for the adsorbate of nitrous oxide, the values of  $b_i$  were assumed to be unity. The fractional surface areas calculated from Eqs. (6) and (10) based on the experimental results in Figure 2 are given in Table 2. The integrals in Eqs. (7) and (8) were calculated using a four point Simpson's rule in the temperature range of -78 °C to -45 °C. The points used in the numerical integration are shown in Figures 2 and 3. The fractional catalyst surface areas determined from hydrogen chemisorption are also given in Table 2. The active surface area given in Table 1 was divided by the total surface area to obtain the percent

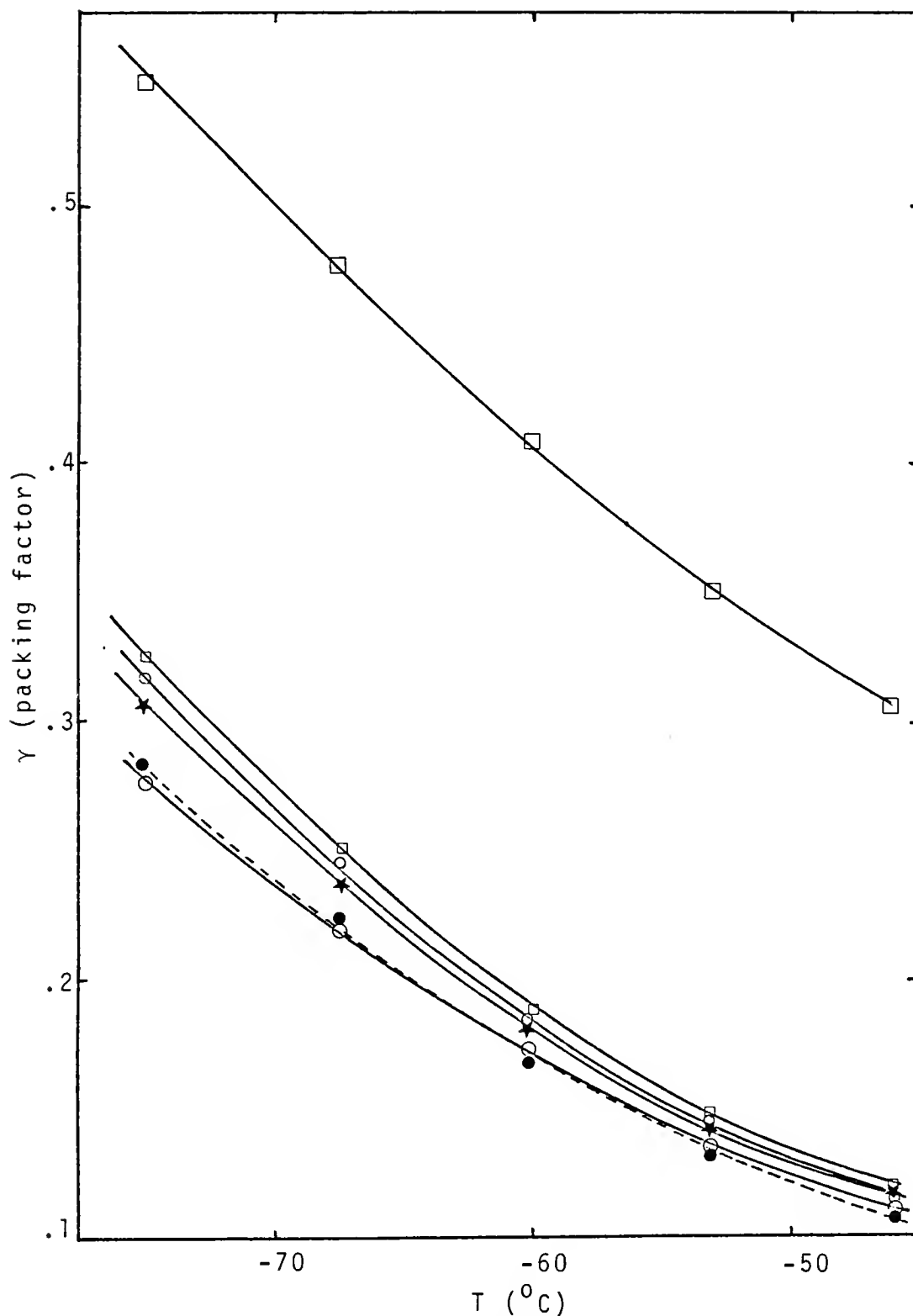


Figure 2. Nitrous oxide selective physisorption on platinum-silica catalyst (normalized curves).

Table 2. Comparison between selective physisorption and hydrogen chemisorption for platinum catalyst supported on silica.

Sample	H <sub>2</sub> chemisorption %Pt Area from	N <sub>2</sub> O physisorption %Pt Area from
1 wt% Pt	5.6	8.6
5 wt% Pt	0.7	-0.9*
10 wt% Pt	5.4	4.9
15 wt% Pt	5.7	6.9

\*This is the actual calculated value which is within the experimental error and should be considered as 0%.

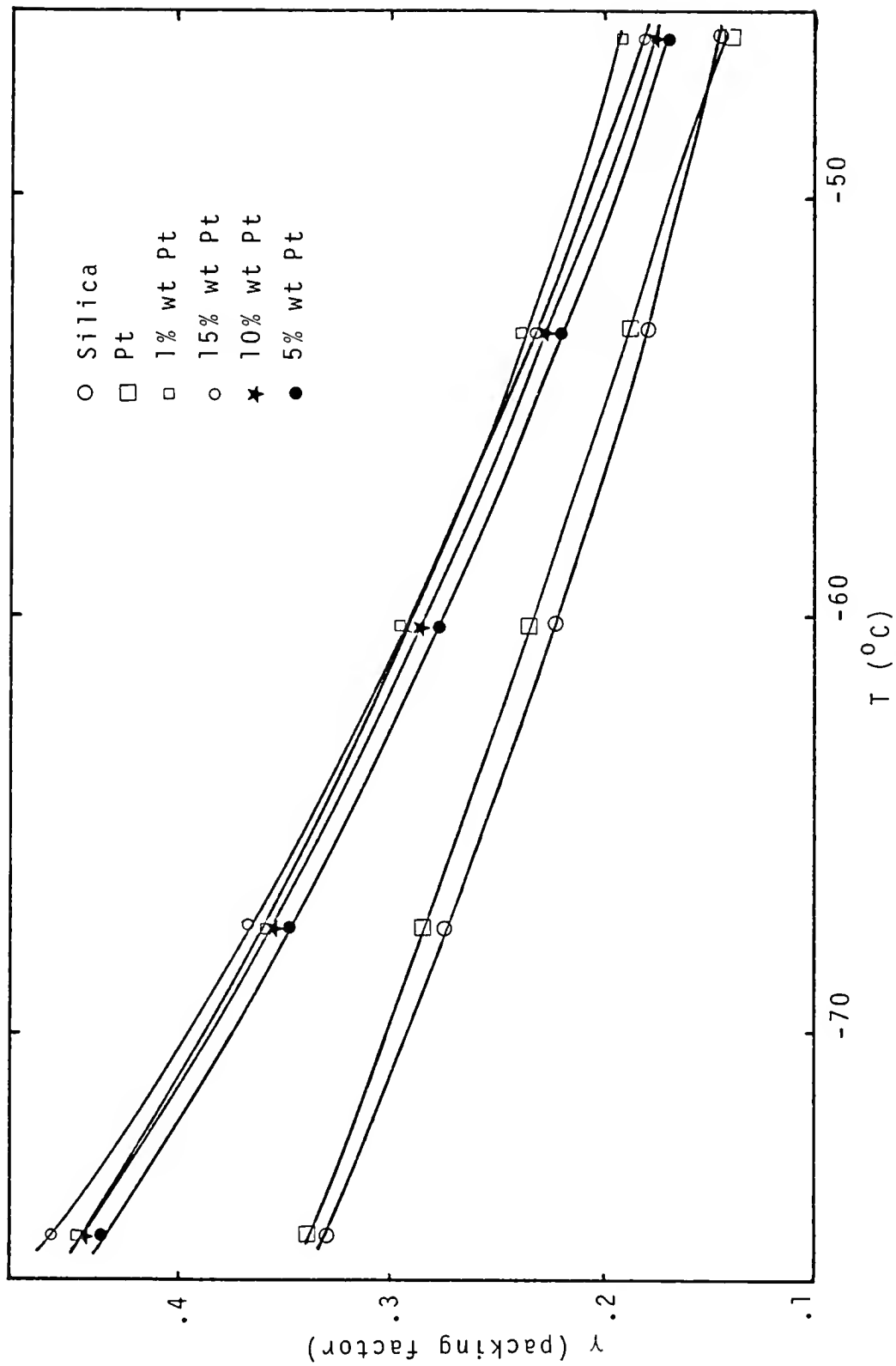


Figure 3. Carbon dioxide selective physisorption on platinum-silica catalyst (normalized curves).



platinum area given in Table 2 under the heading  $H_2$  chemisorption.

The comparison made in Table 2 between chemisorption and selective physisorption shows that for the higher loading samples (5, 10, 15 wt%Pt), the selective physisorption results for the percent platinum area compare well with the chemisorption results, i.e. -0.9% (0%) versus 0.7%, 4.9% versus 5.4%, and 6.9% versus 5.7% for 5, 10, 15 wt%Pt catalysts respectively. The comparison for the 1 wt%Pt catalyst (8.6% versus 5.6%) is not, however, as good as for the higher loading catalyst samples. The crucial test for the selective physisorption method was whether it can distinguish between .7% and 5.7% platinum surface area in a reproducible manner, especially when the total surface areas are as small as 0.037 and 0.324  $m^2/g_{cat}$ , respectively. While the selective physisorption results are not as accurate as hydrogen chemisorption is for platinum-silica catalysts, the comparison shows that it can still distinguish the difference between small variations of active catalyst surface areas. This finding is significant in light of the fact that there are at present no experimental methods that can give such an accuracy for supported metal base oxide catalysts, for which the selective physisorption is intended. This is also true for some metal catalysts, as indicated by the attempts of Miller and Lee (1984) with X-ray diffraction/small angle scattering and SEM/TEM

techniques for the surface areas of potassium carbonate supported on carbon and silver supported on fused alumina.

If an independent method is available for comparison as in the case of platinum catalyst, it is easy to determine whether the chosen adsorbate is indeed inert to set  $b_i$  equal to unity since the comparison would allow this determination. For the supported catalysts for which an independent method is not available, the definition of  $b_i$  can be used to determine whether the chosen adsorbate is suitable for the selective physisorption method, i.e. whether the adsorbate is inert enough such that  $b_i=1$ . According to the definition of the  $b_i$  (Eq. (10)), the adsorbate should not distinguish between pure and dispersed solids when  $b_i=1$ . Thus,  $v_t/S_t$  should be the same if  $b_i = 1$  whether it is for a physical mixture or a supported catalyst as long as  $S_1/S_t$  is the same for both. For a chosen adsorbate for a given catalyst, therefore, one can first assume that  $b_i = 1$  and then calculate  $S_1 / S_t$  from Eqs. (6), (11), and (12). Using this calculated value of  $S_1 / S_t$ , a physical mixture of the two components constituting the supported catalyst can then be prepared and  $v_t / S_t$  obtained experimentally. A comparison between  $v_t/S_t$  thus determined and  $v_t / S_t$  obtained experimentally should reveal whether the chosen adsorbate is suitable for the supported catalyst. The better sensitivity afforded by the use of  $\gamma$ -T relationship rather than  $\theta$ -T relationship is illustrated in Figure 4 for the platinum catalyst being considered. As was the case in Figure 1, The

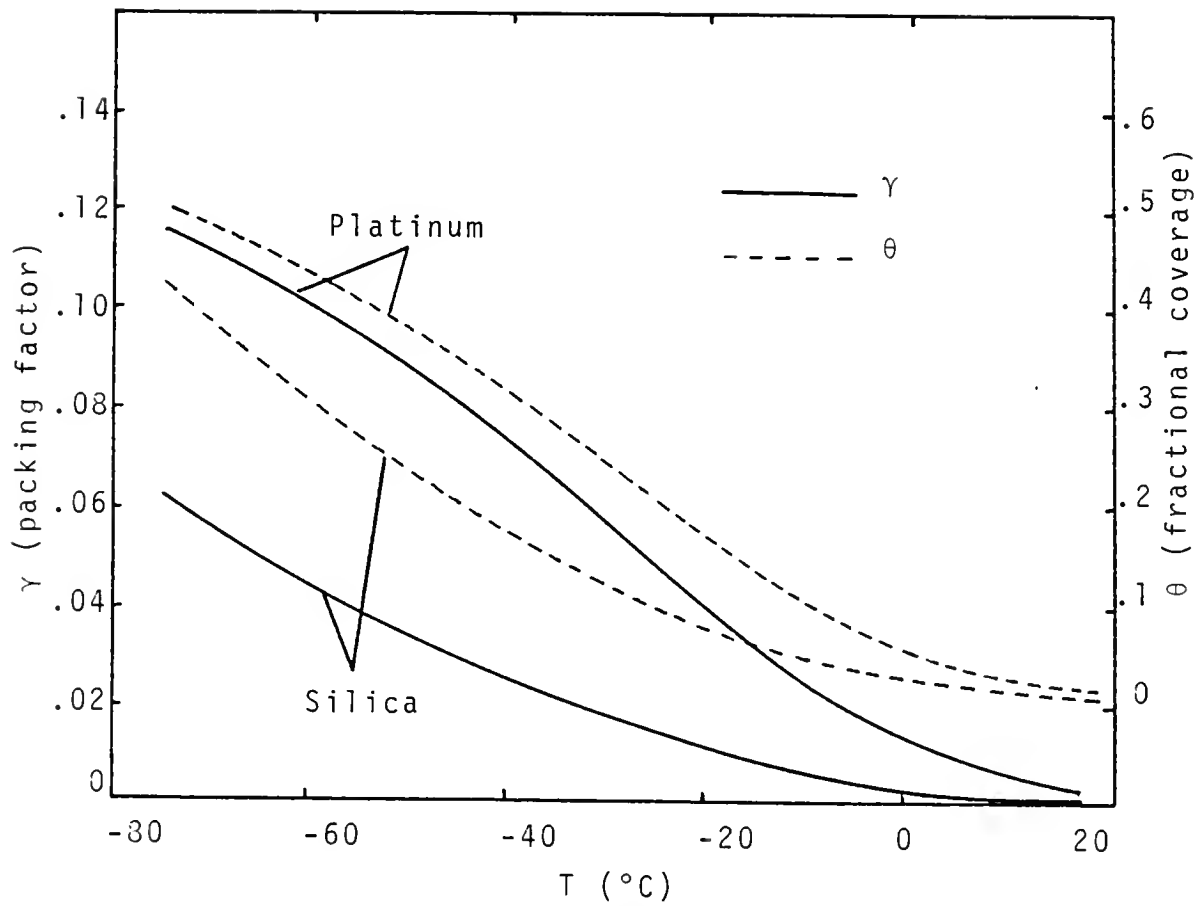


Figure 4. Comparison between the  $\gamma$ - $T$  curves and the  $\theta$ - $T$  curves for the platinum silica system.

use of the packing factor leads to a spread between the pure components larger than that for the  $\theta$ -T relationship and thus a more accurate determination of the fractional surface area of the catalyst.

The results shown in Figure 3 for the adsorbate carbon dioxide immediately reveal that carbon dioxide is not a suitable adsorbate for the supported platinum catalyst. The results also reveal that  $b_i$  cannot be unity since the curves do not lie between the  $\gamma_1$  and  $\gamma_2$  curves. Nevertheless, the results are quite intriguing in that carbon dioxide does not distinguish between pure platinum and pure silica and yet it distinguishes between supported catalysts of different loadings as evident from the different  $\gamma_t$  curves shown in Figure 2. This finding suggests that the selective physisorption of carbon dioxide could be used as a probe for studying the platinum catalyst since the amount of chemisorbed hydrogen is the same regardless of dispersion whereas the amount of selectively physisorbed carbon dioxide per unit surface area of the catalyst depends on dispersion.

The work of Miller and Lee (1984) with carbon dioxide and the results presented here with nitrous oxide fortify the earlier contention that an adsorbate exhibiting a large asymmetric directional polarizability is a good candidate for the selective physisorption method. According to the directional polarizabilities tabulated by Ross and Oliver

(1964), carbon disulfide, acetylene, and benzene should also be considered for selective physisorption in addition to nitrous oxide and carbon dioxide.

#### CHAPTER 4

### APPLICATION OF THE SELECTIVE PHYSISORPTION METHOD TO OXIDE CATALYSTS

As mentioned earlier, the main advantage of the method of selective physisorption will be a more general application to a wider variety of catalysts. If a suitable adsorbate is selected the new method should be equally applicable to metal, metal oxide and metal compound catalysts. It should be noted that although selective chemisorption has been very successfully applied to many metal catalysts it has not been effective on some other metal catalysts. The situation is even worse in the case of metal compound and metal oxide catalysts, where the chemisorption method has had only limited success, and a considerable amount of research is still being done to determine the fractional catalyst surface area of these catalysts. In this chapter we present the application of nitrous oxide selective physisorption to determine the fractional catalyst surface area of two industrially important oxide catalysts namely: (1)  $\text{MoO}_3 / \text{Al}_2\text{O}_3$ , and (2)  $\text{MoO}_3 / \text{SiO}_2$  catalyst. Since no reliable independent method of measuring the fractional surface area of these catalysts is available to date, a verification of the results similar to the one carried out for the platinum silica catalyst using hydrogen chemisorption is not possible. Therefore the results of the selective physisorption

method for these catalysts will be verified by correlating them with the cyclohexane dehydrogenation activity measured with the help of a differential fixed bed reactor.

### Experimental Apparatus

The apparatus used for the selective physisorption of nitrous oxide on the oxide catalysts was identical to the one used earlier for the metal catalyst except that the thermal conductivity detector was replaced by a new Gow Mac Temperature Regulated Cell Assembly. The new detector is equipped with a temperature controller to control the temperature of the detector and allows a much higher bridge current to be used which renders the system much more sensitive.

A differential bed plug flow reactor was used to determine the catalytic activity of the oxide catalyst for the dehydrogenation of cyclohexane. A schematic diagram of the reaction apparatus is given in Figure 5. The tubular reactor was made of 12 mm quartz tube and had a length of 40 cm. Spherical joints, also made of quartz, were placed at both ends of the reactor tube to allow ease of loading of the catalyst samples and cleaning of the reactor tube. A chromel alumel thermocouple was placed on the outside wall of the reactor tube and right above the differential catalyst bed, to measure the reaction temperature. The reactor tube and the thermocouple were wrapped tightly with a half inch wide heating tape (Electrothermal Engineering Limited) which was covered by a few layers of fiber glass insulating tape

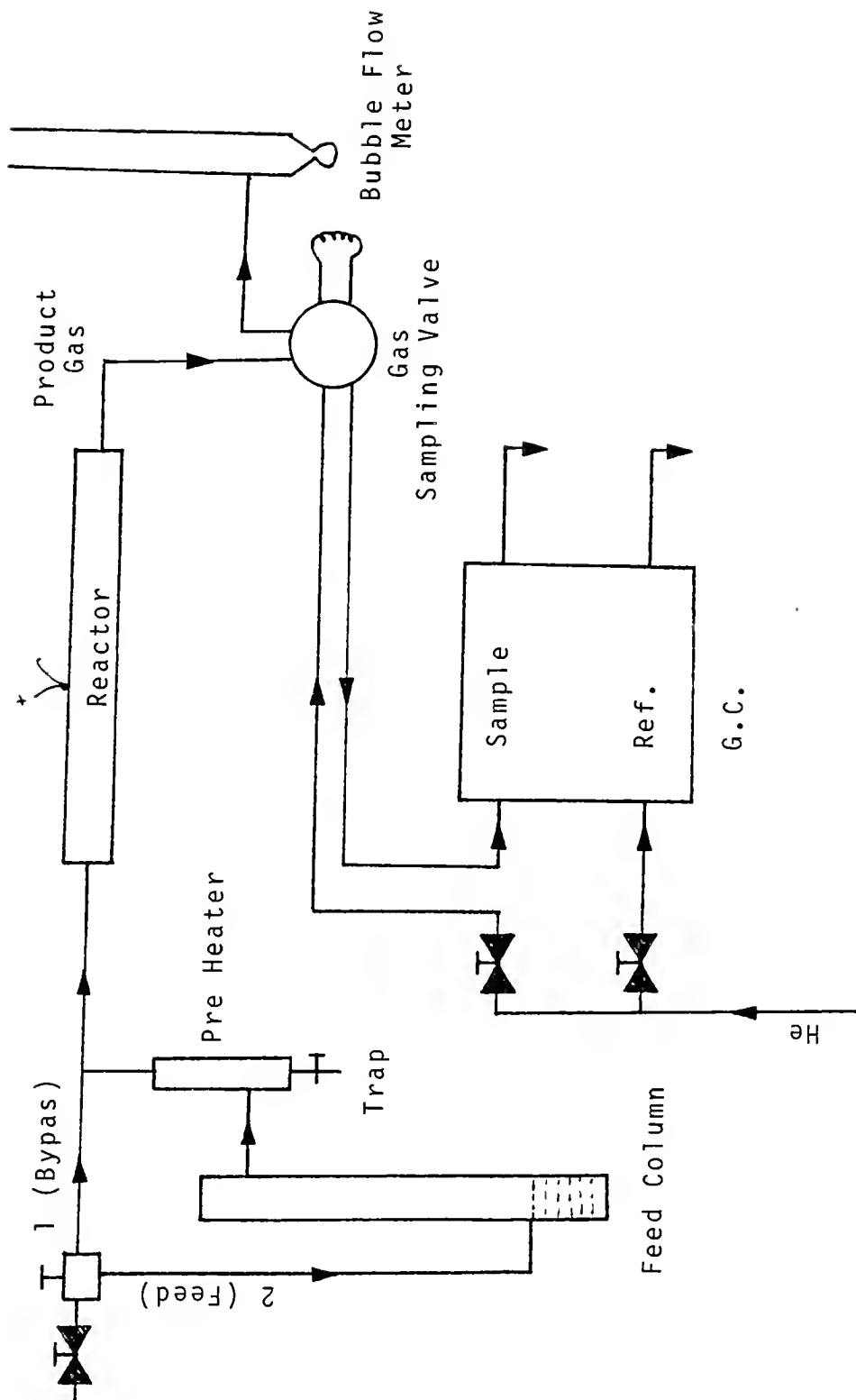


Figure 5. Schematic diagram of the differential reactor.



followed by about one and half inches of fiber glass insulation blanket. The two ends of the heating tape were connected to a variable power supply which was manually regulated to control the reactor temperature at 425 °C. Each catalyst sample was 0.5 to 1.0 gram in size and was secured from both sides by about 1.5 cm long bed of pyrex wool.

The catalyst sample was loaded into the reactor tube to ensure that all samples would be located at the same point inside the reactor, right below the location of the thermocouple placed on the outside wall of the reactor tube. To do this a small bed of pyrex wool was first pushed in through the inlet side of the reactor with the help of a one foot long glass rod. A weighed amount of catalyst sample was then added to the reactor and secured from the other side with the help of another piece of pyrex wool. This piece of pyrex wool was pushed into the reactor tube to ensure a snugly packed bed of catalyst. Excess force was not used in order to avoid a very tightly packed catalyst bed which may cause higher pressure drops and/or channeling of the feed gas. After the catalyst had been loaded the spherical joints at the two ends of the reactor tube were connected to the respective gas lines and secured with the help of pinch clamps. A very small amount of silicon grease (Dow Corning) was applied to the joints to ensure leak free connections.

Nitrogen gas (Linde, Ultra High Purity, 99.999%) was used as the inert carrier in the reactor. The nitrogen pressure was set at 10 psig from the pressure regulator on the

gas cylinder and was never disturbed throughout the experiments. A needle valve was used to regulate the inert carrier flow while the downstream by-pass valve was kept at position 1 (reactant feed column by-pass) in the Figure 5. The gas flow rate was measured with the help of a soap bubble meter provided at the down stream end of the product gas line. Once the carrier flow had been adjusted the needle valve was not disturbed until all the catalysts had been processed.

A specially designed reactant feed column, also shown in Figure 5, was used to feed cyclohexane vapor to the reactor. The bottom part of the 12 mm diameter pyrex column was filled with liquid cyclohexane at room temperature. The cyclohexane liquid level was brought up to a premarked level before starting the reaction with each catalyst sample. Nitrogen carrier gas was introduced in the feed column just above the liquid surface to sweep the cyclohexane vapor inside the feed column and exit at the top end of the reactor. This arrangement was used to avoid excessive entrainment of cyclohexane which might result if a bubble column were used. Before this design was adopted a bubble column was used to saturate the carrier gas with cyclohexane vapor. The result was a very high entrainment of cyclohexane in the feed gas. Every effort was made to avoid excessive entrainment or to remove the entrained liquid from the feed gas but with little success. The entrained liquid would settle in the feed lines and the concentration of the reactant would

continue to increase and not stabilize even after several hours of operation. The entrainment problem was eliminated when the feed gas was introduced above the surface of the liquid reactant as described above.

The feed column was immediately followed by a liquid trap which was equipped with a teflon stopcock at the bottom, to purge any liquid that may settle at the bottom of the trap. The upper portion of the liquid trap was used as a preheater which was heated by a coil of insulated nichrome wire wrapped on the out side of the glass tube. In the center of the preheater was a 2 mm thick glass frit which was used to ensure proper heating of the feed stream. The feed gas was then transmitted to the quartz reactor through a 1/8 inch polyethylene tubing which was insulated with fiber glass tape on the outside.

The product line from the differential reactor was passed through a six port zero volume stainless steel gas sampling valve (Supelco, model 2-2915) mounted on the sample side of the gas chromatograph and then vented through a soap bubble meter into the fume hood. A 0.25 ml stainless steel sample loop (Supelco, model 2-2640) was used with the gas sampling valve to take samples of the product stream for analysis.

A Hewlett Packard model 5790A series gas chromatograph equipped with a thermal conductivity detector was used for the analysis of the reaction products. The gas connections in the original chromatograph were altered to install a six

port zero volume stainless steel gas sampling valve (Supelco, model 2-2915) on column A of the gas chromatograph which was used for the sample gas. The gas sampling valve was mounted right above the column oven and connected directly to the chromatographic packed column bypassing the injection port on the column A. This was done in order to maintain the length of metal tubing between the gas sampling valve and the packed column because a long tubing could cause excessive peak broadening and thus introduce error.

The reaction products were separated with the help of a 1/8 in. X 6 foot stainless steel column (Supelco) packed with di-n-decylphthalate on Chromosorb P (20 wt%) (Maggiore et al., 1979). The column oven was programmed from 130 °C to 160 °C at a rate of 4 °C/min followed by a 6.5 min isothermal operation at 160 °C. The detector temperature and the temperature of the injection port were kept at 250 °C. These conditions were chosen after many trial runs to get sharp separation of the product peaks at the fastest rate.

A Hewlett Packard model 3790A reporting integrator was used to record the thermal conductivity cell response from the chromatograph. The integrator was attached to the chromatograph with the help of a remote starter cable in order to synchronize the run of the chromatographic oven with that of the integrator. Helium (Linde, Ultra High Purity, 99.999%) was used as the carrier gas in the chromatograph, and was further purified by passing through a molecular sieve trap (4 °A, Davison) for the removal of water. The

helium flow rate was kept at 20 ml/min through both the reference and the sample sides of the chromatograph. The nitrogen gas used as the inert carrier in the differential reactor was purified by passing through a bed of activated carbon (American Scientific Products) followed by a bed of 13x molecular sieve (American Scientific Products) to remove hydrocarbons and moisture respectively. The flow rate of the gas in the reactor was about 10 ml/min.

### Experimental Procedure

The chromatograph was started in accordance with the instructions given in the operator's manual for the hewlett packard 5790A series chromatograph. The helium supply pressure was set at 50 psig from the gas cylinder and the flow rate of the gas adjusted to 20 ml/min using the flow regulator valves provided on the front panel of the chromatograph and with the help of the soap bubble meter. After the carrier flow rate had stabilized the column oven was turned on and its temperature brought to 130 °C mark. The detector temperature was then set at 250 °C and the system allowed to stabilize for eight to ten hours. In addition to this at least one temperature programmed run was made on the chromatograph before processing any samples of the product gas to clean the packed columns. The detector current was turned on at least two hours before conducting any experiments to allow sufficient time for the system to stabilize. For overnight shut downs the detector sensitivity was either lowered or turned off to protect the detector elements from

excessive wear and tear. The thermal conductivity detector output was calibrated with the help of  $1 \times 10^{-3}$  ml injections of a standard mixture of cyclohexane and benzene. Another  $1 \times 10^{-3}$  ml injection of deionized distilled water was used to calibrate the  $H_2O$  peak.

Each catalyst sample was dried for six to ten hours depending on whether it was powdered or in the form of pellets. Without this drying time excessive amount of  $H_2O$  would be detected in the product stream. Visual observation determined that the moisture released from the catalyst, pores upon heating in the reactor tube, would settle in the uninsulated spherical quartz joint at the end of the quartz reactor and then continue to humidify the effluent gas stream at a very slow rate. Nevertheless, six hours of drying was sufficient to remove all the moisture and the drying was considered to be complete when no moisture was detected in the product gas. It must be mentioned that the drying was carried out at the reaction temperature and in an inert helium environment. Also, since the drying temperature was lower than the calcination temperature of  $500^\circ C$ , it is believed that this procedure did not effect other properties of the catalyst. It is believed that the only effect of drying was the removal of moisture from the surface of the catalyst.

After drying, the carrier bypass valve was switched to position number 2 in the Figure 5. Thirty minutes were allowed for the reaction to stabilize before taking the

first sample for analysis. It took 18.7 min for the chromatographic oven to complete one run and return to the ready state again. The following run was started as soon as the oven returned to the ready state. A total of four runs was made for each catalyst sample.

### Catalyst Preparation

Five catalyst samples of moly-alumina catalyst with 0.1, 5, 10, 15, 25 wt%MoO<sub>3</sub> per gram of catalyst were prepared by impregnating high surface area alumina (Norton, SA-6173; 1/16 in pellets) with an aqueous solution of ammonium molybdate (Fisher; A-674). Deionized distilled water (4.4 ml/5 gal alumina) was used to to prepare the impregnating solution. The amount of ammonium molybdate used for a particular catalyst was calculated to give the desired loading of MoO<sub>3</sub> on alumina. The actual amounts of the salt and water used are given in the appendix. The aqueous solution prepared was just enough to completely saturate the support material. Care was taken to ensure that very little excess solution remained in the crucible after all the solution had been added, and at the same time no alumina pellets were allowed to be left dry. The system was then allowed to stand for 22 hours followed by 24 hours of drying in the oven at 110 °C. The dried samples were transferred to a high temperature furnace where the catalysts were calcined in air for 17 hours at a temperature of 500 °C. After calcination the samples were allowed to cool in air and then they were

transferred to glass sample bottles for storage. The total weight of each sample prepared was 20 gm.

Five catalyst samples of moly-silica catalyst with 0.1, 5, 10, 15, 20 wt%MoO<sub>3</sub> loading per gram of silica were also prepared in the same way as the moly-alumina catalysts. High surface area silica catalyst support (Alfa, 80396) was impregnated with an aqueous solution of ammonium molybdate. Deionized distilled water (12.5 ml/5 g silica) was used to prepare the impregnating solution. The actual amounts of the salt and water used for each catalyst are given in the appendix. Impregnation was allowed to continue for 24 hours. The catalyst seemed almost dry at the end of the impregnation period but was dried further for 24 hours in an oven at a temperature of 110 °C. Calcination in air was carried out for 18 hours in a furnace at 500 °C. The calcined sample was crushed to obtain a uniform powder and was stored in glass sample bottles.

### Experimental Results And Discussion

Nitrogen BET was used to determine the surface area of each catalyst using the continuous flow sorptometer. The results indicate that molybdenum oxide is present in the form of a monolayer on the surface area of alumina for up to 15wt%MoO<sub>3</sub> loading catalyst. That is to say that the dispersion of MoO<sub>3</sub> is very close to unity in the case of the 5, 10, and 15 wt%MoO<sub>3</sub> loading catalysts. The 25 wt%MoO<sub>3</sub> loading moly-alumina catalyst is believed to carry MoO<sub>3</sub> crystallites and its behavior is therefore different from the lower



loading  $\text{MoO}_3$  loading moly-alumina catalysts. In the case of the moly-silica catalysts the BET results suggest the formation of  $\text{MoO}_3$  crystallites for even the 5 wt% $\text{MoO}_3$  loading catalyst. A detailed discussion of the BET results for the moly-alumina and moly-silica catalysts follows.

The BET surface areas of the moly-alumina catalysts are given in Table 3. Figure 6 shows the decrease of total catalyst surface area of different moly-alumina catalysts as the  $\text{MoO}_3$  loading is increased. However, if the total surface area of the individual catalysts is calculated per gram of alumina, it is seen that it remains constant for the 5, 10, and 15 wt% $\text{MoO}_3$  catalysts, and then increases significantly for the 25 wt% $\text{MoO}_3$  catalyst. This observation that the total surface area per gram of alumina for the 5, 10, and 15 wt% $\text{MoO}_3$  loading moly-alumina catalysts remains constant, is consistent with published data (Liu and Weller, 1980). It conforms to the monolayer model for the moly-alumina catalysts which suggests that in the unreduced catalyst molybdenum oxide is present in the form of an epitaxial monolayer on the surface of alumina. The monolayer model for the unreduced moly-alumina catalyst is a widely accepted model in the published literature (Massoth, 1973). Massoth, for instance, has used butene chemisorption at 100 °C on freshly prepared 10 wt% $\text{MoO}_3$  loading moly-alumina catalyst to show a butene to molybdena ratio of 0.63 which compares well with his theoretical value of 0.64 obtained by assuming that all the molybdena were available on the surface for

Table 3. Nitrogen BET surface area of moly-alumina catalyst.

wt% MoO <sub>3</sub>	Area	
	m <sup>2</sup> /gcat	m <sup>2</sup> /galumina
0.1	164.0	166.0
5.0	172.1	181.0
10.0	163.0	181.0
15.0	152.7	180.0
25.0	154.0	204.0

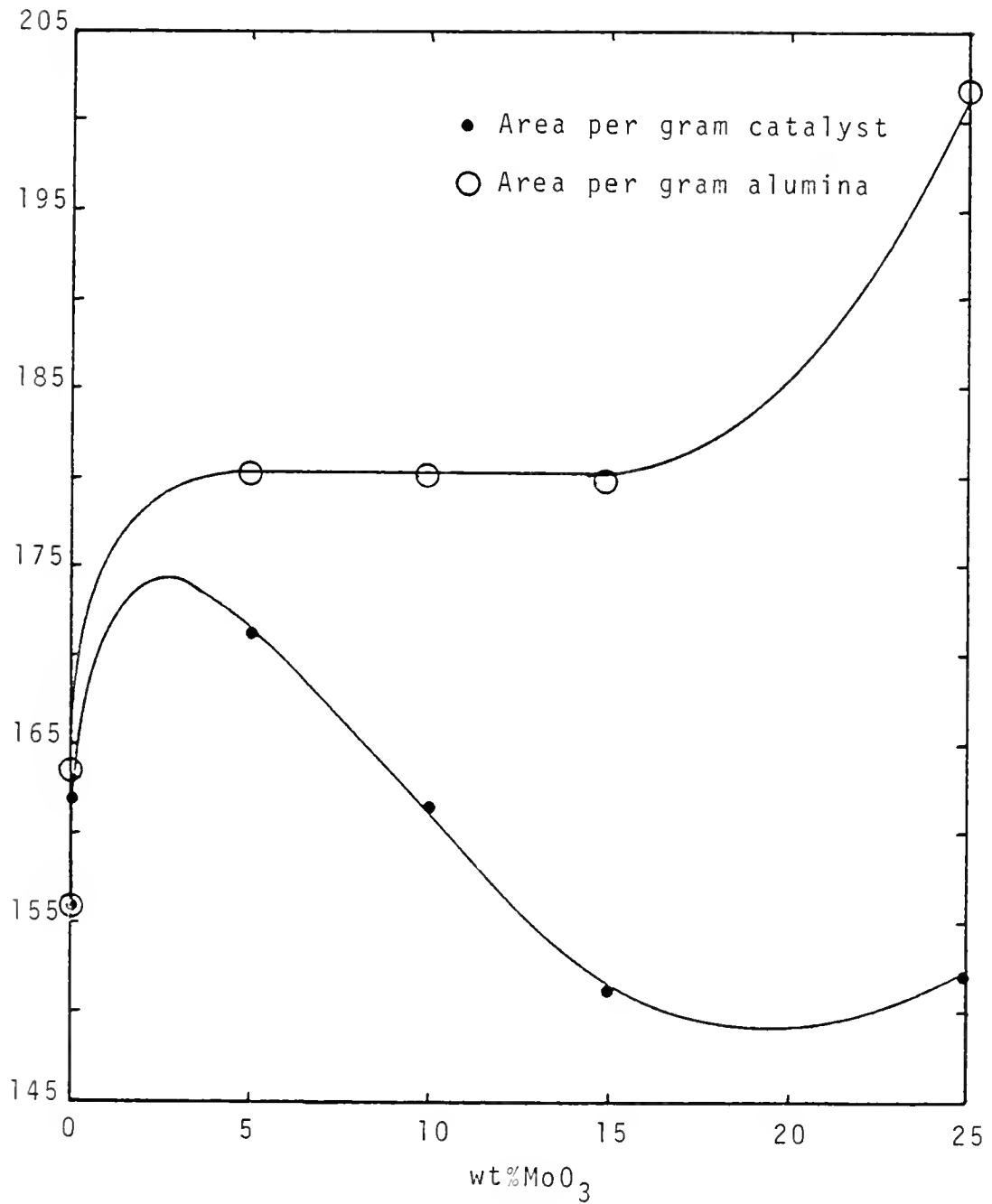


Figure 6. BET surface area of moly-alumina catalyst.

adsorption. Massoth has also observed that only the 25 wt%MoO<sub>3</sub> loading catalyst gave a sharp XRD peak for MoO<sub>3</sub>, suggesting that crystalline moly is present only in the higher loading moly-alumina catalysts. Stencel et al. (1983) have studied MoO<sub>3</sub>/Al<sub>2</sub>O<sub>3</sub> with the help of Raman Spectroscopy and XRD. Their results also show that crystalline MoO<sub>3</sub> is present only in the higher loading moly-alumina catalysts. Therefore we conclude that the increase in the BET surface area (per gram of alumina) for the 25 wt%MoO<sub>3</sub> loading moly-alumina catalyst is due to the presence of crystalline moly which contributes to the total surface area of the catalyst. For the catalysts with up to 15 wt%MoO<sub>3</sub> loading the molybdenum oxide appears to form an epitaxial monolayer on the surface of alumina.

The BET results for the moly-silica catalyst are given in Table 4. It is seen that the total surface area of the moly-silica catalysts decreases with increased MoO<sub>3</sub> loading. This can be explained by viewing the structure of the moly-silica catalyst which is quite different from that of the moly-alumina catalyst. No substantial evidence in the literature was found which may suggest the formation of a monolayer on the surface of silica. In fact, Garcia Fierro et al. (1980) have shown the presence of MoO<sub>3</sub> crystallites on the surface of silica for a 13 wt%MoO<sub>3</sub> loading moly-silica catalyst with the help of a SEM micrograph. Even though the total surface area of the moly-silica catalyst remained constant for Garcia Fierro et al., in all the

Table 4. Nitrogen BET surface area of moly-silica catalyst.

wt% MoO <sub>3</sub>	Area	Area
	m <sup>2</sup> /gcat	m <sup>2</sup> /gsilica
0.1	318.6	318.6
5.0	252.0	265.3
10.0	222.0	246.7
15.0	174.0	204.7
20.0	159.4	199.3

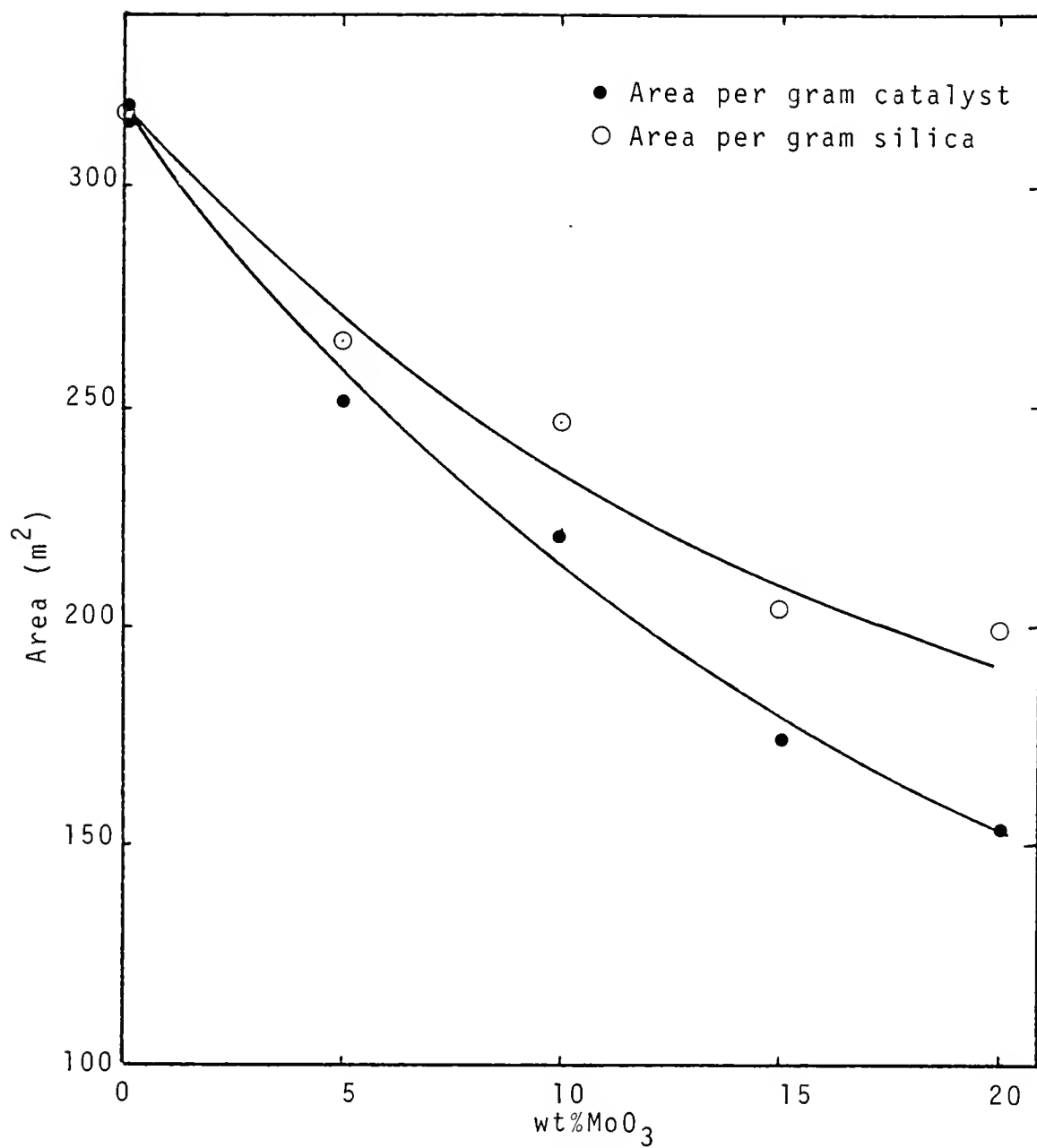


Figure 7. BET area of moly-silica catalyst.

catalysts the total surface area of the catalyst was much less than the area that should have been contributed by the amount of silica support present in the catalyst samples. In addition to this the pore volume of their catalyst also decreased from  $1.34 \text{ cm}^3 / \text{gm}$  for silica to 1.03, 0.86, and  $0.75 \text{ cm}^3 / \text{gcat}$  for the catalysts containing 4.8, 8.1 and 13.0 wt%MoO<sub>3</sub>, respectively. Thus it was concluded that the MoO<sub>3</sub> crystallites block the pores in silica and this results in reduced surface area of the catalyst as the MoO<sub>3</sub> loading is increased. This is in contrast to the behavior exhibited by the 25 wt% moly-alumina catalyst where the MoO<sub>3</sub> crystallites contributed to the total surface area of the catalyst. However, it may be recalled that the alumina used in the moly-alumina catalyst was in the form of pellets and its pore size distribution may be different from the pore size distribution of the silica used in the moly-silica catalyst. Thus, while the moly crystallites may block the pores of silica they may not block the pores of the alumina used in the moly-alumina catalyst.

The results of nitrous oxide selective physisorption indicate that nitrous oxide is not the ideal adsorbate for the moly-alumina catalyst if the absolute value of the fractional surface area is of interest. Also it is observed that the values of the proportionality constants  $b_i$  in Eq. (10) cannot be unity for the nitrous oxide selective physisorption on the moly-alumina catalyst. Therefore, nitrous oxide selective physisorption cannot be used to determine

the absolute value of the fractional catalyst surface area of moly in the moly-alumina catalysts. Nevertheless, as will be seen latter, ratios of the fractional surface areas of different moly-alumina catalysts with up to 15 wt%MoO<sub>3</sub> loading can still be evaluated with the help of nitrous oxide selective physisorption data. In the case of the moly-silica catalyst, it was found that nitrous oxide selective physisorption does not yield any useful information regarding the fractional catalyst surface area. A detailed discussion of these results follows.

The results of nitrous oxide selective physisorption at -78 °C on the MoO<sub>3</sub>/Al<sub>2</sub>O<sub>3</sub> catalyst, and the MoO<sub>3</sub>/SiO<sub>2</sub> catalyst are shown in Figures 8 and 9, respectively. Each data point shown in these two figures represents the average of the two experimental values obtained for each catalyst sample being considered. The error analysis indicates that the values of the packing factors may be  $\pm 2\%$  in error (Appendix F). In light of this fact the differences between the  $\gamma_t$  values of the 5, 10, and 15 wt%MoO<sub>3</sub> loading moly-alumina catalysts (about 2% each) may not seem to be significant. However, it was noted that the maximum scatter in the experimental data for any individual catalyst never exceeded 1.6% and in most cases was less than 1.0%. Also, because the difference between the minimum and the maximum  $\gamma_t$  values is much greater than 2%, we believe that the differences shown are indeed significant and the trend shown by the data is real.



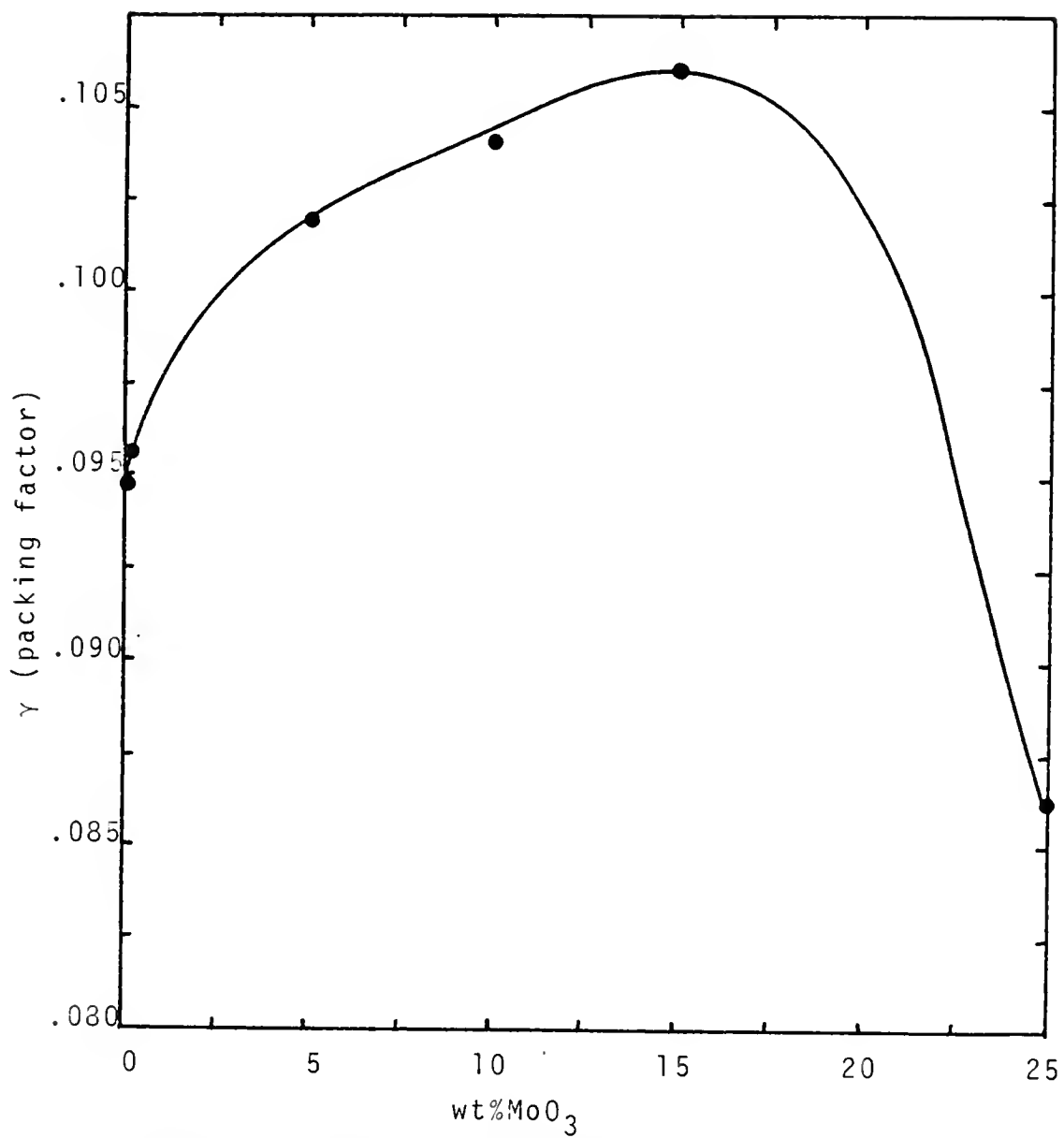


Figure 8. Nitrous oxide selective physisorption on moly-alumina catalysts.

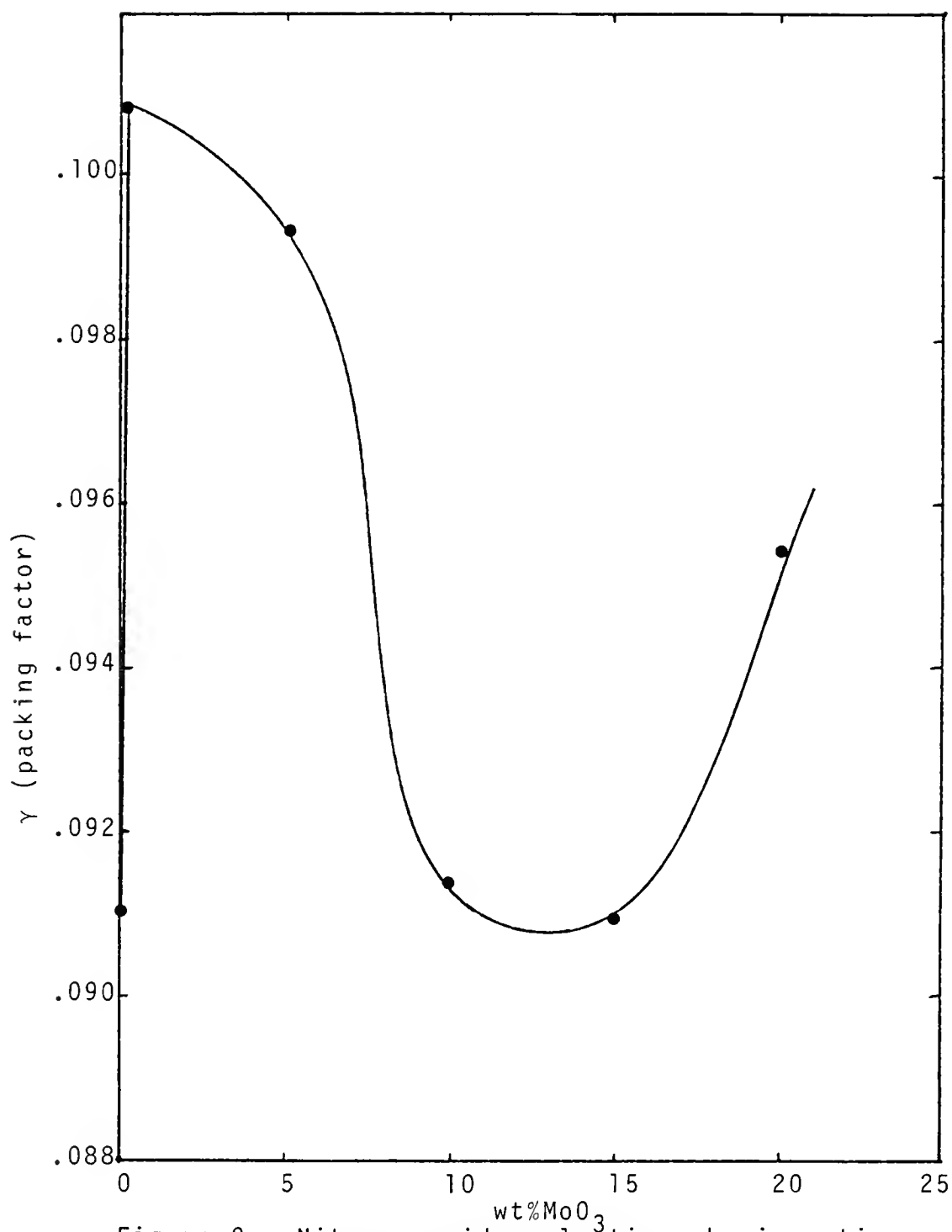


Figure 9. Nitrous oxide selective physisorption on moly-silica catalyst.

In Figure 8 it is seen that the nitrous oxide packing factor for the moly-alumina catalyst increases with increased  $\text{MoO}_3$  loading with up to 15 wt% $\text{MoO}_3$  loading, and then decreases sharply for the 25 wt% $\text{MoO}_3$  loading catalyst. This behavior can be explained by viewing the different structure of the higher loading catalyst. As it was discussed earlier, the molybdenum oxide in the 25 wt% $\text{MoO}_3$  catalyst appears to be present in the form of  $\text{MoO}_3$  crystallites along with the one present as  $\text{Al}_2(\text{MoO}_4^{2-})_3$  (Massoth, 1973). Since the packing factor for the pure  $\text{MoO}_3$  is much less than the packing factor for pure alumina the  $\text{MoO}_3$  crystallites in this catalyst may force the value of the packing factor for the 25 wt% $\text{MoO}_3$  loading catalyst to move towards the pure  $\text{MoO}_3$  value. Thus the packing factor for the 25 wt% $\text{MoO}_3$  loading catalyst is much lower than those of the lower loading moly-alumina catalysts. Because of this complexity, the theory of selective physisorption cannot be rigorously applied to the 25 wt% $\text{MoO}_3$  catalyst.

For the lower loading moly-alumina catalysts, it is clear that the packing factors for the dispersed catalysts are higher than the packing factors for the pure components. Therefore the  $b_i$  in Eq. (10) cannot be unity for selective physisorption of nitrous oxide on the moly-alumina catalyst. In order to get any meaningful results from these data we assume that the catalyst with 0.1 wt% $\text{MoO}_3$  loading has negligible fractional catalyst surface area. Considering that the total surface area of the individual catalysts is of the

order of  $170 \text{ m}^2/\text{gcat}$ , this assumption does not seem to be unrealistic. In that case then, the  $0.1 \text{ wt\%MoO}_3$  catalyst may be considered as the pure support with  $b_2$  equal to unity. Therefore, from Eq. (10) we get

$$R_1 x_1(T) = b_1 \gamma_1(T) \quad (13)$$

and

$$R_2 x_2(T) = \gamma_2(T). \quad (14)$$

Substituting these expressions in Eq. (5) for catalysts  $j$  and  $k$

$$\left[ \frac{s_1}{s_t} \right]_j = \frac{1 - \left[ \frac{v_t}{s_t} \right]_j \left[ \frac{1}{\gamma_2(T)} \right]}{1 - \left[ \frac{b_1 \gamma_1(T)}{\gamma_2(T)} \right]} \quad (15)$$

and

$$\left[ \frac{s_1}{s_t} \right]_k = \frac{1 - \left[ \frac{v_t}{s_t} \right]_k \left[ \frac{1}{\gamma_2(T)} \right]}{1 - \left[ \frac{b_1 \gamma_1(T)}{\gamma_2(T)} \right]}. \quad (16)$$

Divide Eq. (15) by Eq. (16) to get

$$\frac{\left[ \frac{s_1}{s_t} \right]_j}{\left[ \frac{s_1}{s_t} \right]_k} = \frac{1 - \left[ \frac{v_t}{s_t} \right]_j \left[ \frac{1}{\gamma_2(T)} \right]}{1 - \left[ \frac{v_t}{s_t} \right]_k \left[ \frac{1}{\gamma_2(T)} \right]} \quad (17)$$

which can be used to calculate the ratios of the fractional catalyst surface areas of different catalysts. The results of this calculation for the moly-alumina catalysts are given in Table 5. Thus even in the case where  $b_i$  are not unity it is possible to at least evaluate the ratios of the fractional surface areas of different wt% loading catalysts using a catalyst with negligible wt% loading as pure support.

Theoretical values of fractional surface area ratios of different moly-alumina catalysts, calculated by assuming a complete monolayer formation of  $\text{Al}_2(\text{MoO}_4^{2-})_3$  and a  $\text{MoO}_4^{2-}$  cross section of 25 Å (Massoth, 1973), are also given in Table 5. It is seen that the theoretical values do not compare well with the experimental values. Also, if indeed the monolayer model for the moly-alumina catalyst were valid, and in light of the fact that the analysis of the BET results does point towards the formation of an epitaxial monolayer of molybdenum on the surface of alumina, the results of the theoretical calculation should not be very far from the actual values of the fractional surface area ratios. On the other hand, it must be born in mind that the theoretical calculations only represent an upper limit for the fractional surface area ratios and the calculated values are only hypothetical in nature. In any event, it is clear that the values calculated from the nitrous oxide selective physisorption are much lower than the theoretical values.

Table 5. Ratios of fractional surface areas of  
moly alumina catalysts.

Method	$\frac{(S_1/S_t)_{15}}{(S_1/S_t)_5}$	$\frac{(S_1/S_t)_{10}}{(S_1/S_t)_5}$	$\frac{(S_1/S_t)_{15}}{(S_1/S_t)_{10}}$
N <sub>2</sub> O Physisorption	1.69	1.33	1.27
Monolayer Model	3.4	2.1	1.6

Since little is known about the stoichiometry of the interactions between the selectively physisorbed gas and the catalyst surface, we are unable to explain as to why the nitrous oxide selective physisorption results are much lower than the theoretically calculated values of the fractional surface area ratios. Nevertheless, it is interesting to note that the results of the two calculations follow the same trend. It may also be pointed out that the fractional surface area of a 15 wt%MoO<sub>3</sub> moly-alumina catalyst obtained by Parekh and Weller (1977), using low temperature oxygen chemisorption, was also about one fourth of the value that may be obtained if a monolayer model were adopted. From this discussion it is clear that more work needs to be done in order to understand and explain the reason for the disagreement between the results of the nitrous oxide selective physisorption and the theoretical results obtained by assuming molybdenum monolayer on the surface of alumina. Since there is no other independent method available to measure the fractional surface area of the oxide catalysts, an absolute verification of the nitrous oxide selective physisorption method was not possible. Therefore, in order to make a qualitative comparison, it was decided to compare the cyclohexane dehydrogenation activity of the oxide catalysts with the nitrous oxide packing factors obtained from the selective physisorption of nitrous oxide.

The nitrous oxide selective physisorption results for the moly-silica system do not yield any useful information

regarding the fractional surface area of the catalyst. At best the packing factors for the moly-silica catalysts of different wt%MoO<sub>3</sub> loadings show a decreasing trend up to 15 wt%MoO<sub>3</sub> loading catalyst, but due to the more complex nature of this catalyst a better explanation cannot be offered at present. The sudden increase in the value of the packing factor for the 20 wt%MoO<sub>3</sub> loading moly-silica catalyst is not understood.

The cyclohexane dehydrogenation experiments were carried out in a differential reactor and the results for the moly-alumina catalyst system and the moly-silica catalyst system are shown in the Figures 10 and 11, respectively. The data shown in these two figures represents the run number two for each catalyst being considered. It may be recalled that four samples of the product gas were analyzed for each catalyst sample. Since a differential reactor was being used it is important to compare the activity of each catalyst after it has been exposed to the same reaction conditions for the same duration of time. The error analysis indicates that the calculated values of the catalyst activity may be +5% in error.

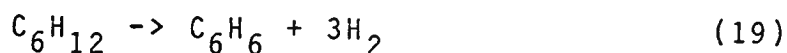
The rate of reaction was calculated from

$$-r_c = F \left[ \frac{\Delta X}{\Delta W} \right] \quad (18)$$

where  $F$  is the molar feed flow rate and  $\Delta X$  and  $\Delta W$  are the differential conversion and the weight of the catalyst,



respectively. Cyclohexane, benzene and water were the only components detected in the product stream. Since the reactor was being operated in differential mode and the amount of coking did not increase significantly with the increased catalyst loading, it was neglected in the calculation of the rate of reaction. The conversion was calculated by assuming the reaction



only. The small amount of the  $\text{H}_2\text{O}$  present in the product stream may be attributed to the water attached to the  $\text{Al}_2(\text{MoO}_4)_3$  species which could have been released upon cyclohexane chemisorption on the surface of the catalyst. It merits mention that the concentration of the  $\text{H}_2\text{O}$  reduced drastically in the first two runs and only trace amount was detected in the subsequent runs, while the concentration of cyclohexane and benzene remained constant in all the runs. This observation fortifies our contention that the  $\text{H}_2\text{O}$  present in the product stream does not represent a product but is merely the water chemisorbed on the catalyst which is released when cyclohexane chemisorption starts.

Figure 10 shows that no reaction was observed on pure alumina or the 0.1 wt% $\text{MoO}_3$  catalyst. After that the rate of reaction increased steadily from 5 wt% $\text{MoO}_3$  to 15 wt% $\text{MoO}_3$  catalyst, and then the rate of increase of the reaction rate slowed down towards the 25 wt% $\text{MoO}_3$  catalyst. It is believed

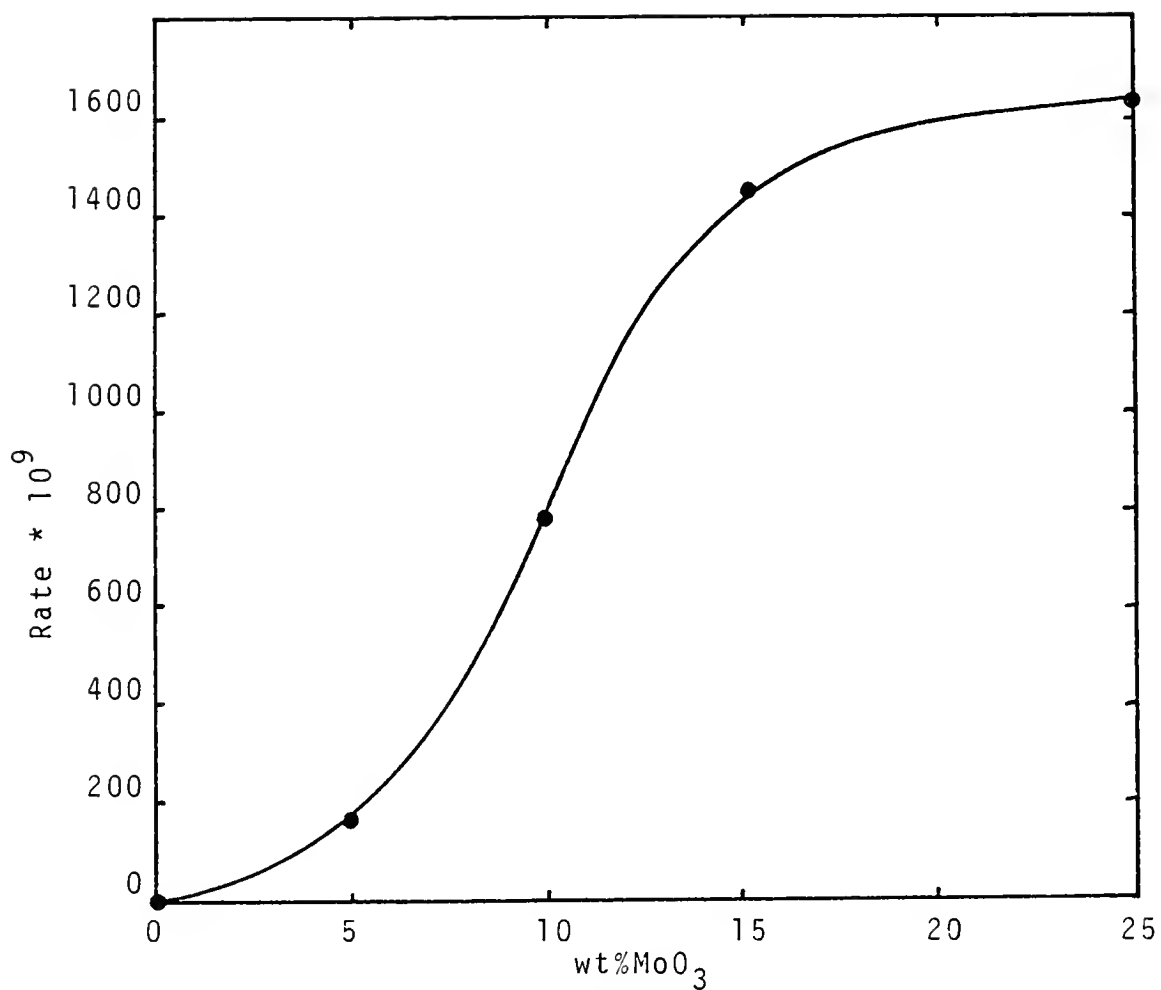


Figure 10. Rate of cyclohexane dehydrogenation on moly-alumina catalysts.

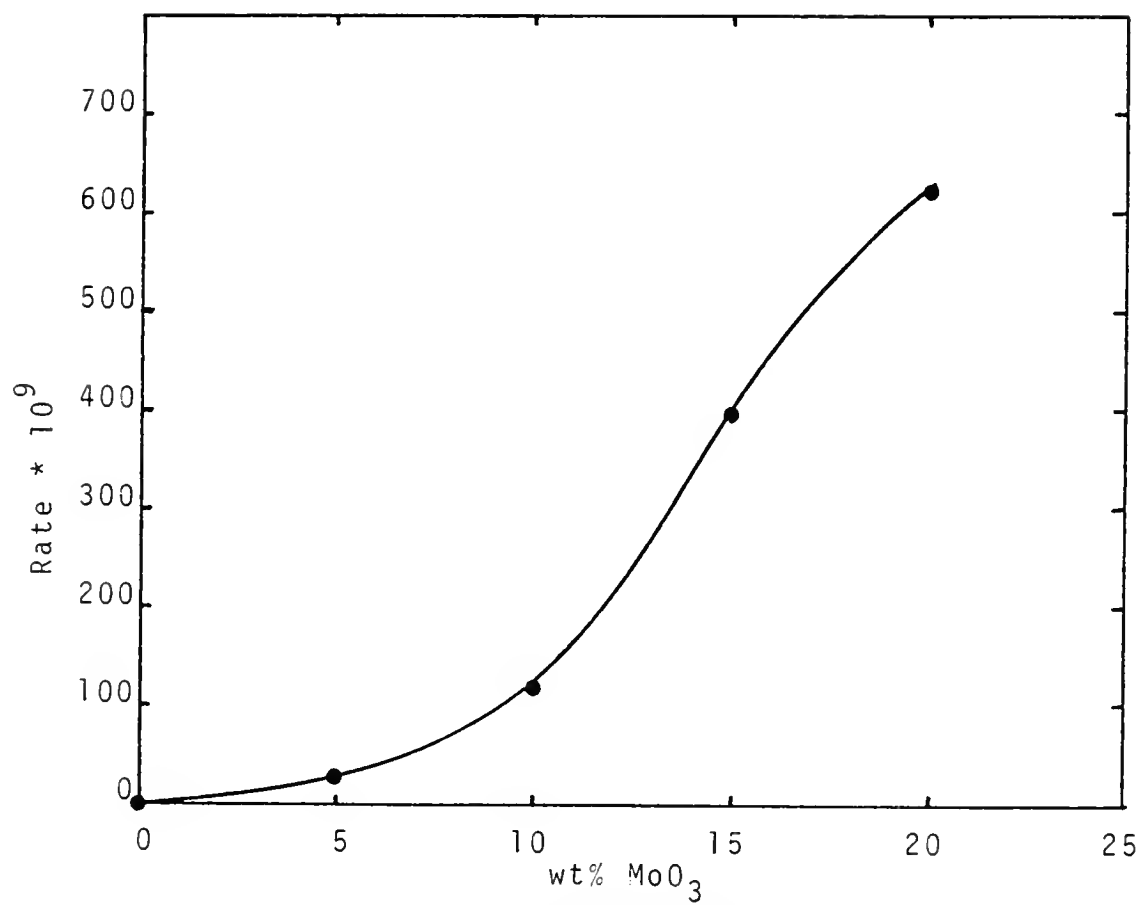


Figure 11. Rate of cyclohexane dehydrogenation on moly-silica catalyst.

that this change in the rate of increase of the reaction rate is primarily due to the change in the nature of the catalyst surface as the loading increases from 15 to 25 wt%MoO<sub>3</sub>. It has been discussed earlier that MoO<sub>3</sub> crystallites may be present on the surface of the 25 wt%MoO<sub>3</sub> catalyst. The present observation further strengthens our belief that the 25 wt%MoO<sub>3</sub> catalyst is different in nature from the lower loading catalysts and, therefore, must be treated separately.

The correlation between the nitrous oxide packing factors and the cyclohexane dehydrogenation activity of the moly-alumina catalysts is shown in the Figure 12. It is seen that the activity increases with the increase in the value of the packing factor. This, however, is not the case for the 25 wt%MoO<sub>3</sub> catalyst but this catalyst has already been shown to be an exception. Again, in spite of the relatively small differences in the individual values for the 5, 10, and 15 wt%MoO<sub>3</sub> catalysts (about 2% each), the correlation is believed to be significant because of the good reproducibility experienced in the selective physisorption experiments and the overall trend of the data. Thus, the correlation shown in the Figure 12 is believed to present a valid partial verification of the nitrous oxide selective physisorption results.

In the case of the moly-silica catalyst also, the cyclohexane dehydrogenation activity is seen to increase with increased MoO<sub>3</sub> loading (Figure 11). Also, as in the

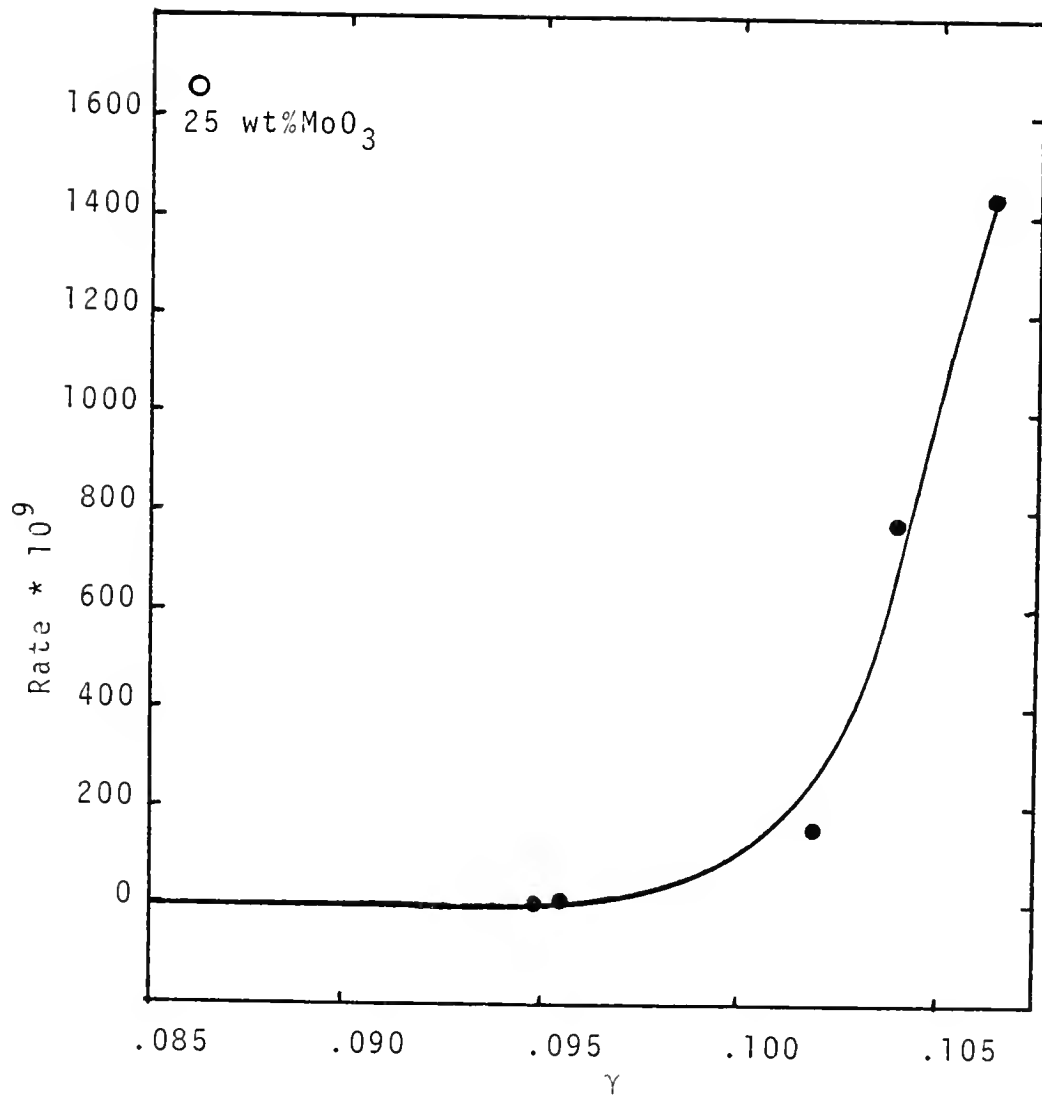


Figure 12. Correlation between cyclohexane dehydrogenation and nitrous oxide packing factors for moly-alumina catalyst.

case the moly-alumina catalyst, no reaction was observed on pure silica or the 0.1 wt%MoO<sub>3</sub> catalyst. The rate of reaction increased steadily with increase in the MoO<sub>3</sub> loading and no shift in behavior was observed for the higher loading catalyst. This observation along with the BET results shown in the Figure 6 leads us to believe that all moly-silica catalysts may be similar in nature in the sense that all crystalline MoO<sub>3</sub> may be present even in the lower loading catalysts. No useful correlation between the activity of cyclohexane dehydrogenation and the nitrous oxide selective physisorption results could be obtained for the moly-silica catalysts. Therefore we conclude that nitrous oxide selective physisorption does not provide any useful information regarding the fractional catalyst surface area of the moly-silica catalyst system.

In order to further study the moly-alumina catalyst surface, the 10 wt%MoO<sub>3</sub> catalyst was analyzed using X-ray photoelectron spectroscopy. The survey scan for the 10 wt%MoO<sub>3</sub> catalyst is shown in the Figure 13. The positioning of the individual peaks on the binding energy scale can be adjusted for the experimental work function by taking the Al 2p peak as the reference peak. According to the data given in the handbook of X-ray photoelectron spectroscopy (Wagner et al., 1979), the binding energy of the Al 2p peak for Al<sub>2</sub>O<sub>3</sub> is 74.1-74.3 eV, and the binding energy of the Al 2p peak for Al<sub>2</sub>(MoO<sub>4</sub><sup>2-</sup>) is 74.4 eV. Since only a fraction of the total aluminum may be present as Al<sub>2</sub>(MoO<sub>4</sub><sup>2-</sup>)<sub>3</sub>, the Al 2p

peak is moved to 74.2 eV which is the average value of the binding energy for  $\text{Al}_2\text{O}_3$ . This gives an experimental work function of 4.85 eV. Using this experimental work function value the binding energies of the Mo 3d, O 1s, and C 1s peaks come out to be 232.85 eV, 531.4 eV, and 278.9 eV, respectively. It is interesting to note that the binding energy of the Mo 3d peak (232.85 eV) is very close to the the binding energy of the Mo 3d peak for  $\text{Al}_2(\text{MoO}_4^{2-})_3$  (232.8 eV). Also, since the binding energies for  $\text{MoO}_3$  and  $\text{MoO}_2$  are less than 232.7 eV, we may conclude that Mo is present on the catalyst surface as  $\text{Al}_2(\text{MoO}_4^{2-})_3$ .

A high resolution scan of the C 1s peak is shown in the Figure 14. The binding energy of the C 1s peak suggests that the carbon is present in the form of a carbide. A definitive source of the surface carbon is not known. However, the carbon may partially be present due to carbon dioxide and carbon monoxide present in the atmosphere which may have chemisorbed on the catalyst surface upon exposure to the air. It is quite likely that during calcination the chemisorbed carbon oxides left some graphitic carbon on the catalyst surface which in turn transformed into a carbide.

The surface composition of the 10 wt% $\text{MoO}_3$  moly-alumina catalyst obtained from the X-ray photoelectron spectroscopy data is given in Table 6. It is seen that carbon represents 3.37 mass% of the total catalyst surface. However, it is not clear whether the carbon is present on the catalyst surface in the form of a thin monolayer or in the form of large

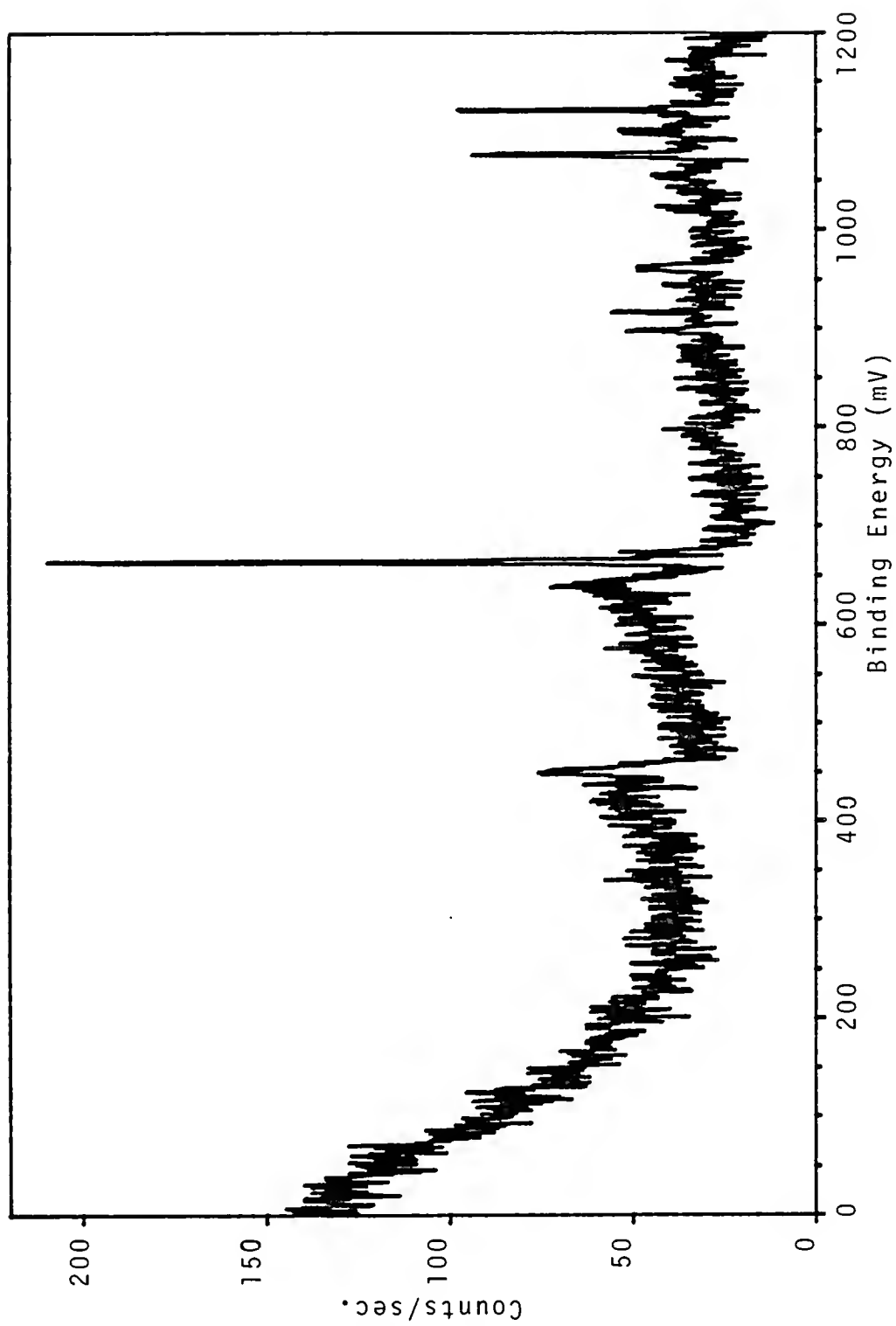


Figure 13. X-ray photoelectron spectroscopy survey scan for the 10 wt%MoO<sub>3</sub> moly-alumina catalyst.



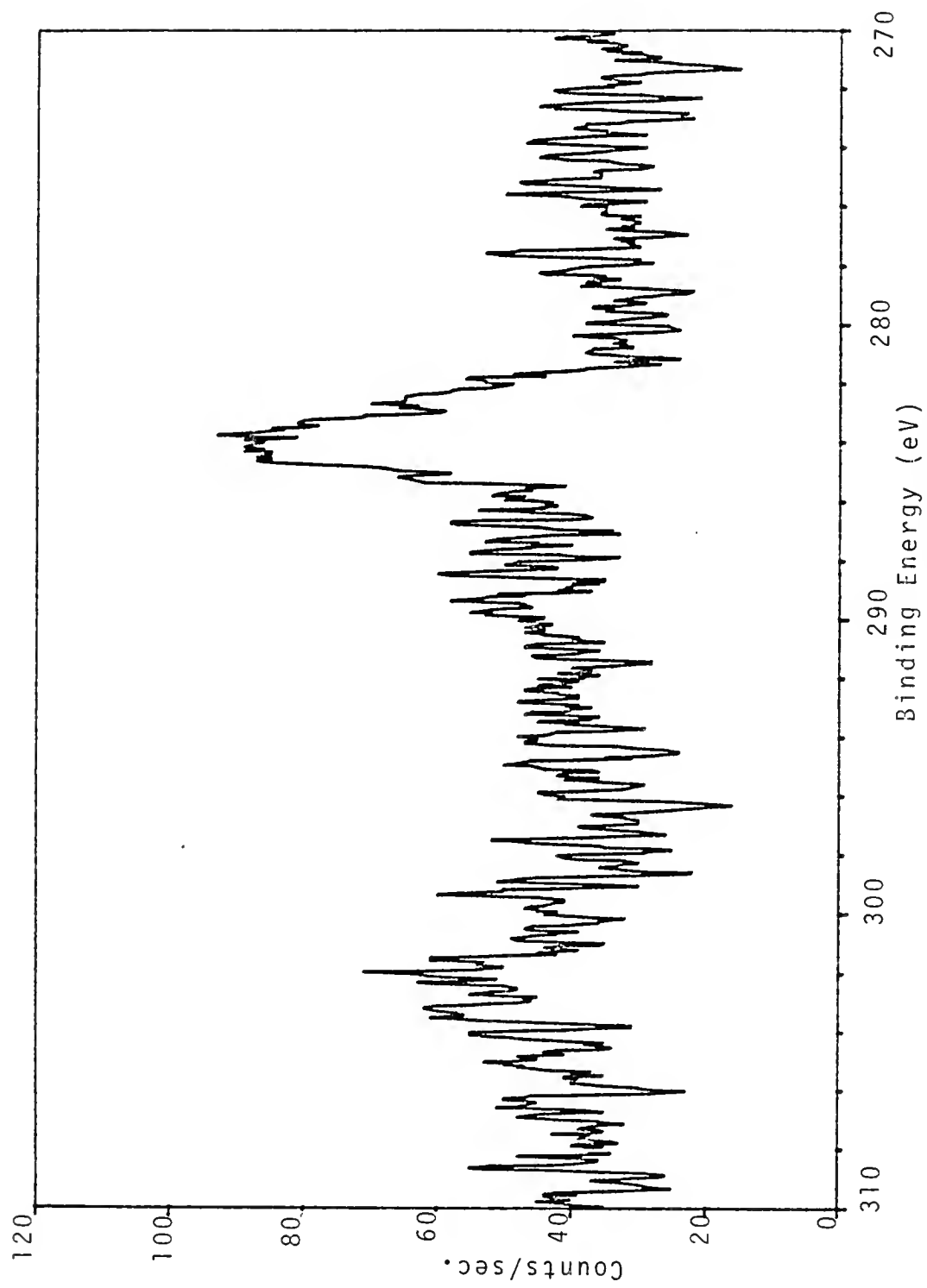


Figure 14. High resolution scan of the carbon peak.

Tabl3 6. Composition of the 10 wt%MoO<sub>3</sub> moly-alumina catalyst as obtained from the x-ray photo-electron spectroscopy data.

Element	Position	Width	Area	Quant		Mass	
				Factor	Ratio	Conc %	
Al 2p	74.2	3.45	591	0.29	7.35:1	55.72	
Mo 3d	232.85	3.70	442	4.51	0.351:1	9.46	
O 1s	531.4	3.50	1671	0.86	7.001:1	31.45	
C 1s	278.9	1.85	138	0.49	1:1	3.37	

crystallites. Also it is not known as to how the presence of this carbon may effect the nitrous oxide selective physisorption on the catalyst because similar carbon may be present on all the catalyst samples as well as the two pure components. Therefore, we recommend a thorough investigation of these aspects when future work is undertaken. It will be important to identify, with certainty, the source and form of the surface carbon so that the effects of carbon on the method of selective physisorption can be evaluated. Identification of the source may also aid in avoiding the carbon deposit if that is deemed essential for the method of selective physisorption to be effective.

#### Summary

The method of selective physisorption for measuring the fractional catalyst surface area of dispersed catalysts has been applied to the oxide catalysts with moderate success. Five moly-alumina catalysts of different  $\text{MoO}_3$  loading and five moly-silica catalysts of different  $\text{MoO}_3$  loading were prepared by impregnating high surface area alumina and high surface area silica respectively, with aqueous solutions of ammonium molybdate. The total surface area of each catalyst sample was determined with the help of nitrogen BET method. The results of the BET study indicate the formation of a molybdenum oxide monolayer on the surface of alumina for the lower  $\text{MoO}_3$  loading catalysts. That is to say that the dispersion of molybdenum oxide on the surface of alumina is unity for the 5, 10, and 15 wt% $\text{MoO}_3$  catalysts, and is less

than unity for the 25 wt%MoO<sub>3</sub> catalyst. This conclusion was drawn from the observation that the total surface area of the 5, 10, and 15 wt%MoO<sub>3</sub> loading moly-alumina catalysts remains constant when it is calculated per gram of alumina present in the catalyst. This behavior and the subsequent conclusion is consistent with the view of most other researchers in the literature who have studied the moly-alumina system. The increase in the BET surface area of the 25 wt%MoO<sub>3</sub> moly alumina catalyst is attributed to the presence of MoO<sub>3</sub> crystallites on the surface of this catalyst. The MoO<sub>3</sub> crystallites have been confirmed to exist on the higher MoO<sub>3</sub> loading moly-alumina catalyst, with the help of XRD and Raman spectroscopy.

The nitrous oxide selective physisorption was applied to the moly-alumina catalyst. It was observed that the nitrous oxide packing factors for the moly-alumina catalysts increased with increased MoO<sub>3</sub> loading for up to 15 wt%MoO<sub>3</sub> loading catalyst, and then decreased sharply for the 25 wt%MoO<sub>3</sub> loading moly-alumina catalyst. Also it was observed that the nitrous oxide packing factors for the moly-alumina catalysts with up to 15 wt%MoO<sub>3</sub> loading are greater than the nitrous oxide packing factors for the pure MoO<sub>3</sub> and pure alumina. Thus it was clear that nitrous oxide was not the best suited adsorbate for the moly-alumina catalyst if the absolute value of the fractional catalyst surface area is of interest. Nevertheless, ratios of the fractional catalyst surface areas of different catalysts with different wt%MoO<sub>3</sub>

loading can be computed if the 0.1 wt%MoO<sub>3</sub> loading catalyst were considered as the pure component. The underlying assumption here was that the 0.1 wt%MoO<sub>3</sub> loading moly-alumina catalyst has negligible molybdenum oxide surface area and therefore could be used as a reference. Thus the fractional surface area ratios were computed to be 1.3, 1.6, and 1.2 for 10 wt% to 5 wt%, 15 wt% to 5 wt%, and 15 wt% to 10 wt % MoO<sub>3</sub> loading moly-alumina catalysts, respectively. Since the surface characteristics of the 25 wt%MoO<sub>3</sub> loading moly-alumina catalyst are very different from the rest of the catalysts it could not be included in the above calculation. The fractional surface area ratios mentioned above are much lower compared to the theoretical values calculated from the BET results assuming a monolayer of molybdenum oxide on the surface of alumina. However, the results of the two calculations follow the same trend.

The results of nitrous oxide selective physisorption for the moly-alumina catalyst system were substantiated by a correlation between the selective physisorption data and the cyclohexane dehydrogenation activity for the moly-alumina catalysts with up to 15 wt%MoO<sub>3</sub> loading. The 25 wt%MoO<sub>3</sub> catalyst was not included in the correlation because of its different surface characteristics. The correlation is believed to be significant in spite of the relatively small differences in the individual packing factor values because the scatter in the scatter in the experimental values was even smaller. The overall trend of the data also strengthens

this belief. The moly-alumina catalyst was also analyzed using X-ray photoelectron spectroscopy to further study the surface of this catalyst. The results indicate that a substantial amount of carbon is present on the surface of the catalyst in the form of a carbide. The exact source and form of this surface carbon are not yet known with certainty. Also it is not known how this carbon may effect the selective physisorption method. We recommend a more thorough study of this phenomenon in order to develop the method of selective physisorption further.

In contrast to the moly-alumina system the total surface area of the moly-silica catalysts decreased with increased  $\text{MoO}_3$  loading. This was so even when the BET surface area of the catalysts was calculated per gram of silica present in the catalysts. This observation and the results of other researchers led us to believe that  $\text{MoO}_3$  crystallites are present on the moly-silica catalyst even when the catalyst loading is relatively low. The  $\text{MoO}_3$  crystallites block the pores in the silica support and, therefore, the total surface area of the catalysts decreases with increased  $\text{MoO}_3$  loading. The nitrous oxide selective physisorption was not successful in determining the fractional catalyst surface area of the moly silica catalysts. At best a decreasing value of the nitrous oxide packing factor with increased  $\text{MoO}_3$  loading was observed for the moly-silica catalysts with up to 15 wt% $\text{MoO}_3$  loading. This trend reversed for the 20 wt% $\text{MoO}_3$  loading catalyst and the reason for this behavior is

not understood. No correlation could be obtained between the selective physisorption data and the cyclohexane dehydrogenation activity for the moly-silica catalyst system.

## CHAPTER 5 CONCLUSIONS AND RECOMMENDATIONS

The method of selective physisorption for measuring the fractional catalyst surface area of dispersed catalysts as developed by Miller and Lee (1984) has been modified to achieve increased sensitivity towards changes in the fractional surface areas of catalysts with different loadings of the dispersed material. It has been shown that the use of packing factors ( $\gamma$ ) in place of fractional coverage ( $\theta$ ) affords a better sensitivity towards measuring the fractional surface area of any catalyst. The theory has been accordingly modified to incorporate packing factors instead of fractional coverage. A few modifications have also been suggested in the experimental method used for obtaining the adsorption isobars of the selectively physisorbed gas. The new method incorporates the use of more than one constant temperature cold baths to obtain the adsorption isobars and thus eliminates the need for the pseudo steady state assumption that has been used by Miller and Lee (1984). Thus a more dependable adsorption isobar is obtained in this manner.

One important objective of this research was to demonstrate the effectiveness of the method of selective physisorption in measuring the fractional surface area of



supported catalyst, and establish its credibility by using it to determine the surface area of a standard catalyst system. A standard catalyst system would be a one which would provide an already established alternate method of determining its fractional surface area. Platinum dispersed on silica was chosen because the fractional surface area of dispersed platinum can be determined very effectively with the help of hydrogen chemisorption. Four samples of different wt%Pt loading on silica were prepared by impregnating amorphous silica with an aqueous solution of chloroplatinic acid. Both carbon dioxide and nitrous oxide were used to independently determine the fractional surface area of the dispersed platinum in the four catalysts. The results indicate that carbon dioxide is not a suitable adsorbate for measuring the fractional catalyst surface area of platinum in the platinum silica catalyst, although it may provide valuable insight into the said system. Nitrous oxide, on the other hand, was found to be a good adsorbate to be used for the selective physisorption on the platinum silica catalyst. This observation also demonstrated that our earlier contention, that directional polarizability data can be used to select an adsorbate for selective physisorption, was correct.

The values of the fractional surface area of platinum dispersed on silica determined from the selective physisorption of nitrous oxide were found to be in agreement with the values obtained from the hydrogen chemisorption experiments.

It was shown that nitrous oxide selective physisorption is sensitive to even small changes in the platinum surface area as present in the supported catalyst.

In order to advance the method of selective physisorption to metal base oxide catalysts, nitrous oxide selective physisorption was attempted on two industrially important oxide catalysts, namely moly-alumina and moly-silica catalysts. Five samples of each catalyst system were prepared by impregnating high surface area alumina and high surface area silica with aqueous solutions of ammonium molybdate. The total surface area of each catalyst was determined with the nitrogen BET method. The results indicate that the total surface area of up to 15 wt%MoO<sub>3</sub> loading moly-alumina catalysts remained constant when calculated per gram of the alumina present in the catalyst, and the total surface area per gram of alumina of the 25 wt%MoO<sub>3</sub> loading moly-alumina catalyst increased significantly. This observation, along with the data and view of other researchers in the published literature, leads us to the conclusion that moly oxide forms a epitaxial monolayer on the surface of alumina in the moly-alumina catalyst, with up to 15 wt%MoO<sub>3</sub> loading, while crystalline MoO<sub>3</sub> is believed to be present in the 25 wt%MoO<sub>3</sub> loading moly-alumina catalyst along with the moly oxide monolayer.

Nitrous oxide selective physisorption was only partially successful when applied to the moly-alumina catalyst. This is so, because the packing factors for the catalysts

with up to 15 wt%MoO<sub>3</sub> loading were greater in value than the packing factors for the pure MoO<sub>3</sub> and pure alumina. This clearly showed that  $b_1$  for this system could not be unity. Therefore absolute values of the fractional catalyst surface areas of these catalysts could not be determined. Nevertheless, ratios of the fractional surface areas of different moly-alumina catalysts can still be calculated by treating the 0.1 wt%MoO<sub>3</sub> loading catalyst as the pure support. The underlying assumption here is that the fractional catalyst surface area of the 0.1 wt%MoO<sub>3</sub> catalyst is negligible compared to the total surface area of the catalyst. The 25 wt%MoO<sub>3</sub> catalyst was treated as an exception, and was not included in the calculation being discussed here, because it is believed to carry crystalline MoO<sub>3</sub> on its surface which makes the nature of its surface different from the nature of the surface of the catalysts with lower catalyst loadings. The results of this calculation do not compare well with the results of theoretical calculations based on the monolayer model for the moly-alumina catalysts.

An absolute verification of the nitrous oxide selective physisorption results was not possible because no other independent method was available to measure the fractional surface area of the oxide catalyst. Instead a partial verification of results was made using a correlation between the cyclohexane dehydrogenation activity and the nitrous oxide packing factors for the moly-alumina catalysts. The correlation is believed to be significant, in spite of the

relatively small differences between the individual packing factor values, because the scatter in the experimental values was even smaller. The overall trend of the data also suggested that the correlation was indeed significant and valid.

The BET results for the moly-silica catalyst system indicate the presence of  $\text{MoO}_3$  crystallites on the surface of silica which results in decreased total surface area of the catalyst with increased  $\text{MoO}_3$  loading. Nitrous oxide selective physisorption on the moly-silica catalysts was not successful, and it was determined that nitrous oxide is unsuitable for use as an adsorbate for the moly-silica catalyst. No useful correlation could be obtained between the results of nitrous oxide selective physisorption and the cyclohexane dehydrogenation activity of the moly-silica catalysts.

The 10 wt% $\text{MoO}_3$  moly-alumina catalyst was analyzed using X-ray photoelectron spectroscopy to study the surface further. It was observed that in addition to the oxygen, molybdenum, and aluminum present on the surface of the catalyst there was a substantial amount of carbon also present on the surface. The exact source and form of the surface carbon is not yet understood, but the carbon is believed to come from carbon monoxide and carbon dioxide present in the air. Also it is not known how this carbon may effect the selective physisorption method. Therefore, it is recommended that such surface analysis may be included in future work in order to develop the theory of selective

physisorption method further. It will also be important to correctly identify the source of the carbon present on the surface of the catalyst so that it may be avoided if it adversely effects the method of selective physisorption for measuring fractional catalyst surface area.

It is the author's understanding that more work needs to be done to better understand the nature of the interactions between the selectively physisorbed gas and the solid surface. Infra red spectroscopy may be able to offer some insight into the state of the selectively physisorbed gases which will help in establishing a better and more effective criterion for the selection of a suitable adsorbate. Since nitrous oxide selective physisorption was unable to determine the absolute values of the fractional surface areas of the moly-alumina catalysts and nothing for the moly-silica catalysts, we recommend more work in this area. A better adsorbate needs to be selected to obtain more conclusive results. The author suggests acetylene as a suitable candidate for use with the moly-alumina and moly-silica catalyst systems.

An important application of the method selective physisorption may be in studying catalyst deactivation by coking. Preliminary results indicate a large difference between the nitrous oxide packing factors for pure nickel and pure graphite powders. The method may also be helpful in differentiating between the catalyst deactivation caused by

coking and the catalyst deactivation caused by sulfur poisoning when the two occur simultaneously.

APPENDIX A  
PREPARATION OF OXIDE CATALYSTS

Table 7. Preparation of moly-alumina catalyst.

wt% MoO <sub>3</sub>	Alumina (gm)	Ammonium Molybdate (gm)	Water (ml)
0.1	19.9786	0.0253	17.58
5.0	19.0033	1.2285	16.7
10.0	18.0000	2.4532	15.8
15.0	17.0044	3.6800	14.96
25.0	15.0005	6.1356	13.5

Table 8. Preparation of moly-silica catalyst.

wt% MoO <sub>3</sub>	Silica (gm)	Ammonium Molybdate (gm)	Water (ml)
0.1	3.9976	0.0045	50.0
5.0	3.8028	0.2467	47.5
10.0	3.6000	0.4912	45.0
15.0	3.3984	0.7376	42.5
20.1	3.2012	0.9858	40.0



APPENDIX B  
NITROUS OXIDE SELECTIVE PHYSISORPTION DATA  
FOR  
PLATINUM-SILICA CATALYST

Table 9. Experimental conditions for nitrous oxide selective physisorption on platinum-silica catalyst.

Helium pressure (in H <sub>2</sub> O)	25.1
Nitrous oxide pressure (in H <sub>2</sub> O)	1.8
Nitrous oxide Flow meter reading	30.0
Attenuation of desorption peak	x1
Attenuation of calibration peak	x4
Volume of calibration gas (cm <sup>3</sup> )	0.179
Area of calibration peak	99.3
Heater voltage (V)	15.
Total flow rate (cm <sup>3</sup> /min)	33.55
Helium flow rate (cm <sup>3</sup> /min)	30.185
Concentration chart speed (in/min)	2
Temperature chart speed (in/min)	0.5

Table 10. Experimental data of nitrous oxide selective physisorption on platinum-silica catalyst.

Sample	Run	Peak Area	K-Type Thermocouple Reading (mV)	Weight (gm)
1.0 wt%	1	74.0	1.73	0.21395
	2	74.7	1.75	
	3	144.7	2.43	
	4	148.8	2.49	
	5	138.6	2.40	
	6	176.0	2.60	
	7	166.9	2.54	
	9	167.9	2.55	
	10	235.5	2.86	
	11	222.4	2.78	
5.0 wt%	1	54.4	1.72	0.18115
	2	55.8	1.74	
	3	104.8	2.41	
	4	111.5	2.47	
	5	123.2	2.56	
	6	139.5	2.66	
	7	167.4	2.85	
	8	168.4	2.87	
	9	171.1	2.92	
10.0 wt%	1	188.2	2.87	0.2012
	2	175.2	2.83	

Table 10--continued.

Sample	Run	Peak Area	K-Type Thermocouple Reading (mV)	Weight (gm)
15.0 wt%	3	181.1	2.83	0.2185
	4	124.2	2.48	
	5	114.0	2.37	
	6	158.3	2.70	
	7	67.7	1.76	
	8	64.7	1.74	
	1	54.9	1.74	
	2	56.2	1.74	
	3	53.9	1.75	
	4	118.9	2.48	
SiO <sub>2</sub>	5	130.9	2.51	0.1971
	6	137.3	2.57	
	7	161.7	2.77	
	8	127.7	2.56	
	9	173.5	2.83	
	10	173.0	2.84	
	1	85.14	1.75	
	2	88.8	1.76	
	3	155.4	2.46	
	4	166.2	2.54	
	5	167.7	2.60	
	6	197.2	2.71	

Table 10--continued.

Sample	Run	Peak Area	K-Type Thermocouple Reading (mV)	Weight (gm)
Pt	7	222.3	2.85	0.39557
	8	225.9	2.85	
	9	226.9	2.88	
	10	232.1	2.91	
	1	46.1	1.73	
	2	43.4	1.70	
	3	72.8	2.47	
	4	68.4	2.41	
	5	75.7	2.67	
	6	74.7	2.63	
	7	76.0	2.60	
	8	71.8	2.56	
	9	72.4	2.51	
	10	73.6	2.57	
	11	84.5	2.82	
	12	85.4	2.85	
	13	85.9	2.86	
	14	86.4	2.90	

APPENDIX C  
NITROUS OXIDE SELECTIVE PHYSISORPTION DATA  
FOR  
THE OXIDE CATALYSTS

Table 11. Experimental conditions.

Helium pressure	4.
Nitrous oxide pressure	3.5
Attenuation of desorption peak	x16
Attenuation of calibration peak	x4
Volume of calibration peak (cm <sup>3</sup> )	0.25
Area of calibration peak	38.5
Concentration chart speed (in/min)	4
Temperature chart speed (in/min)	4
Heater voltage (V)	8.7
Detector current (mA)	80
Detector temperature (°C)	60
Total flow rate (ml/min)	38.61
Helium flow rate (ml/min)	36.62

Table 12. Experimental data for nitrous oxide selective physisorption on moly-alumina catalyst.

Sample	Run	Peak Area	Temperature (°C)	Weight (gm)
5 wt%	2	99.4	-78.	0.1462
	3	98.0	-78.	
10 wt%	1	103.8	-78.	0.1603
	2	105.3	-78.	
15 wt%	1	101.4	-78.	0.1609
	2	99.8	-78.	
25 wt%	1	84.8	-78.	0.1667
	2	85.5	-78.	
0.1 wt%	1	99.4	-78.	0.1626
	2	98.0	-78.	
Al <sub>2</sub> O <sub>3</sub>	1	90.0	-78.	0.1584
	2	91.4	-78.	
MoO <sub>3</sub>	1	4.6	-78.	0.2632
	2	5.2	-78.	

Table 13. Experimental conditions for nitrous oxide selective physisorption on moly-silica catalyst.

---

Helium pressure	3.4
Nitrous oxide pressure	3.0
Attenuation of desorption peak	x32
Attenuation of calibration peak	x4
Volume of calibration peak (cm <sup>3</sup> )	0.25
Area of calibration peak	52.4
Concentration chart speed (in/min)	4
Temperature chart speed (in/min)	4
Heater voltage (V)	8.7
Detector current (mA)	80
Detector temperature (°C)	60
Total flow rate (ml/min)	38.61
Helium flow rate (ml/min)	36.62

---

Table 14. Experimental data for nitrous oxide selective physisorption on moly-silica catalyst.

Sample	Run	Peak Area	Temperature (°C)	Weight (gm)
MoO <sub>3</sub>	1	8.7	-78.	0.2632
	2	8.7	-78.	
SiO <sub>2</sub>	1	97.8	-78.	0.1263
0.1 wt%	1	91.7	-78.	0.1089
	2	91.6	-78.	
20 wt%	1	47.7	-78.	0.1207
	2	48.2	-78.	
	3	47.9	-78.	
15 wt%	1	49.7	-78.	0.1192
	2	49.5	-78.	
10 wt%	1	66.3	-78.	0.1245
	2	66.0	-78.	
5 wt%	1	67.8	-78.	0.1058
	2	68.5	-78.	



APPENDIX D  
NITROGEN PHYSISORPTION RAW DATA

Table 15. BET data for pure platinum powder.

Weight = 0.33540 gm				
Run	1	2	3	4
Helium pressure (in H <sub>2</sub> O)	25.0	25.0	22.1	26.9
Nitrogen pressure (in H <sub>2</sub> O)	0.	0.	5.0	0.
Nitrogen flow meter	29.0	13.5	13.5	0.
Attenuation of desorption peak	x2	x1	x2	x1
Area of desorption peak	45.5, 55.9, 48.3	82.3, 79.7	55.9, 56.7	63.1
Attenuation of calibration peak	x4	x4	x4	x4
Volume of calibration gas (cm <sup>3</sup> )	.5	.2	.5	.5
Area of calibration peak	168.8	65.8	180.4	174.0
Concentration chart speed (in/min)	1	1	1	1
Temperature chart speed (in/min)	.2	.2	.2	.2
$\bar{p}$	.075	.033	.164	.004

Table 16. BET data for sintered silica.

Weight = 0.17400 gm			
Run	1	2	3
Helium pressure (in H <sub>2</sub> O)	22.0	23.7	26.
Nitrogen pressure (in H <sub>2</sub> O)	4.2	2.0	0.
Nitrogen flow meter	48.0	27.0	4.0
Attenuation of desorption peak	x4	x4	x2
Area of desorption peak	135.0	96.4, 93.7	136.0, 138
Attenuation of calibration peak	x4	x4	x4
Volume of calibration gas (cm <sup>3</sup> )	.5	.5	.5
Area of calibration peak	186.0	176.0	168.3
Concentration chart speed (in/min)	1	1	1
Temperature chart speed (in/min)	.2	.2	.2
$\bar{p}$	.170	.073	.010

Table 17. BET data for 15.0 wt% platinum-silica catalyst.

Weight = 0.1925 gm				
Run	1	2	3	4
Helium pressure (in H <sub>2</sub> O)	22.5	20.0	25.8	24.7
Nitrogen pressure (in H <sub>2</sub> O)	5.0	7.0	0.	1.0
Nitrogen flow meter	51.5	52.0	6.0	30.5
Attenuation of desorption peak	x4	x4	x2	x4
Area of desorption peak	94.3, 92.2	117.9, 118.1	124.7, 122.6	83.6, 80.3
Attenuation of calibration peak	x4	x4	x4	x4
Volume of calibration gas (cm <sup>3</sup> )	.5	.5	.5	.5
Area of calibration peak	166.6	206.0	168.2	169.5
Concentration chart speed (in/min)	1	1	1	1
Temperature chart speed (in/min)	.2	.2	.2	.2
$\bar{p}$	.177	.237	.021	.079

Table 18. BET data for 10 wt% platinum-silica.

Weight = 0.1829 gm				
Run	1	2	3	4
Helium pressure (in H <sub>2</sub> O)	21.8	23.1	25.0	25.0
Nitrogen pressure (in H <sub>2</sub> O)	5.0	0.	.3	0.
Nitrogen flow meter	50.0	19.5	25.2	2.5
Attenuation of desorption peak	x4	x4	x4	x2
Area of desorption peak	98.4, 96.8	86.3, 82.9	85.4, 81.0	124.1, 121.8
Attenuation of calibration peak	x4	x4	x4	x4
Volume of calibration gas (cm <sup>3</sup> )	.5	.5	.5	.5
Area of calibration peak	169.5	182.8	169.2	174.2
Concentration chart speed (in/min)	1	1	1	1
Temperature chart speed (in/min)	.2	.2	.2	.2
$\bar{P}$	.175	.056	.068	.011

Table 19. BET data for 5 wt% platinum-silica catalyst.

Weight = 0.15855 gm				
Run	1	2	3	4
Helium pressure (in H <sub>2</sub> O)	22.1	23.7	25.0	26.0
Nitrogen pressure (in H <sub>2</sub> O)	4.1	2.2	0.	0.
Nitrogen flow meter	46.5	35.5	20.5	0.
Attenuation of desorption peak	x4	x4	x4	x2
Volume of gas desorbed	.263	.238	.206	.115
Attenuation of calibration peak	x4	x4	x4	x4
Volume of calibration gas (cm <sup>3</sup> )	.5	.5	.5	.5
Area of calibration peak	169.1	170.0	170.5	163.2
Concentration chart speed (in/min)	1	1	1	1
Temperature chart speed (in/min)	.2	.2	.2	.2
$\bar{P}$	.165	.109	.050	.005

Table 20. BET data for 1.0 wt% platinum-silica catalyst.

Weight = 0.1715 gm				
Run	1	2	3	4
Helium pressure (in H <sub>2</sub> O)	21.0	23.0	25.0	26.0
Nitrogen pressure (in H <sub>2</sub> O)	4.5	2.0	0.	0.
Nitrogen flow meter	49.5	36.0	22.7	0.
Attenuation of desorption peak	x4	x4	x4	x2
Area of desorption peak	103.9, 100.4	95.0, 91.7	83.4, 82.2 78.8	111.9, 115.5
Attenuation of calibration peak	x4	x4	x4	x4
Volume of calibration gas (cm <sup>3</sup> )	.5	.5	.5	.5
Area of calibration peak	173.8	173.5	169.8	169.6
Concentration chart speed (in/min)	1	1	1	1
Temperature chart speed (in/min)	.2	.2	.2	.2
$\bar{p}$	.179	.110	.061	.012

Table 21. BET data for pure treated alumina.

Weight = 0.19835 gm			
Run	1	2	3
Helium pressure (in H <sub>2</sub> O)	25.8	27.8	29.2
Nitrogen pressure (in H <sub>2</sub> O)	6.9	4.5	2.0
Nitrogen flow meter	50.	41	27
Attenuation of desorption peak	x64	x64	x64
Area of desorption peak	160.5	148,145.7	132.4,132.7
Attenuation of calibration peak	x4	x4	x4
Volume of calibration gas (cm <sup>3</sup> )	.19	.19	.19
Area of calibration peak	57.6	56.4	54.2
Concentration chart speed (in/min)	.5	.5	.5
Temperature chart speed (in/min)	.2	.2	.2
$\bar{p}$	.153	.104	.059



Table 22. BET data for pure moly oxide.

Weight = 0..3575 gm			
Run	1	2	3
Helium pressure (in H <sub>2</sub> O)	26.0	29.1	27.5
Nitrogen pressure (in H <sub>2</sub> O)	6.9	1.8	4.0
Nitrogen flow meter	51.	27.	40.5
Attenuation of desorption peak	x1	x1	x1
Area of desorption peak	58.4, 58.5	44.2, 43.3	51.0, 49.0,
Attenuation of calibration peak	x4	x4	x4
Volume of calibration gas (cm <sup>3</sup> )	.19	.19	.19
Area of calibration peak	56.8	56.2	57.2
Concentration chart speed (in/min)	.5	.5	.5
Temperature chart speed (in/min)	.2	.2	.2
$\bar{P}$	.161	.058	.108

Table 23. BET data for 25 wt% moly-alumina catalyst.

Weight = 0.1750 gm			
Run	1	2	3
Helium pressure (in H <sub>2</sub> O)	26.0	27.6	29.0
Nitrogen pressure (in H <sub>2</sub> O)	7.0	4.5	2.2
Nitrogen flow meter	52	41.	29.
Attenuation of desorption peak	x32	x32	x32
Area of desorption peak	273.5, 270.1	248.4, 244.6	231.7, 231.1
Attenuation of calibration peak	x4	x4	x4
Volume of calibration gas (cm <sup>3</sup> )	.19	.19	.19
Area of calibration peak	57.7	58.0	57.6
Concentration chart speed (in/min)	.5	.5	.5
Temperature chart speed (in/min)	.2	.2	.2
$\bar{p}$	.161	.107	.064

Table 24. BET data for 15 wt% moly-alumina catalyst.

Weight = 0.2563 gm			
Run	1	2	3
Helium pressure (in H <sub>2</sub> O)	26.	27.7	29.2
Nitrogen pressure (in H <sub>2</sub> O)	6.7	4.5	1.5
Nitrogen flow meter	51	42	26
Attenuation of desorption peak	x64	x64	x64
Area of desorption peak	203.2	189.2	175.2
Attenuation of calibration peak	x4	x4	x4
Volume of calibration gas (cm <sup>3</sup> )	.19	.19	.19
Area of calibration peak	58.	56.6	57.
Concentration chart speed (in/min)	.5	.5	.5
Temperature chart speed (in/min)	.2	.2	.2
$\bar{p}$	.158	.112	.060

Table 25. BET data for 10 wt% moly-alumina catalyst.

Weight = 0.2379 gm			
Run	1	2	3
Helium pressure (in H <sub>2</sub> O)	26.0	27.7	29.2
Nitrogen pressure (in H <sub>2</sub> O)	6.6	4.5	1.5
Nitrogen flow meter	51.	42.	27.
Attenuation of desorption peak	x64	x64	x64
Area of desorption peak	194.0	180.	166.7
Attenuation of calibration peak	x4	x4	x4
Volume of calibration gas (cm <sup>3</sup> )	.19	.19	.19
Area of calibration peak	57.4	57.3	58.8
Concentration chart speed (in/min)	.5	.5	.5
Temperature chart speed (in/min)	.2	.2	.2
$\bar{p}$	.151	.113	.062

Table 26. BET data for 5 wt% moly-alumina catalyst.

Weight = 0.2381 gm			
Run	1	2	3
Helium pressure (in H <sub>2</sub> O)	26.0	27.7	29.2
Nitrogen pressure (in H <sub>2</sub> O)	6.8	4.5	1.5
Nitrogen flow meter	51	42.5	26.
Attenuation of desorption peak	x64	x64	x64
Area of desorption peak	207.7	195.2	174.6
Attenuation of calibration peak	x4	x4	x4
Volume of calibration gas (cm <sup>3</sup> )	.19	.19	.19
Area of calibration peak	57.4	55.7	56.3
Concentration chart speed (in/min)	.5	.5	.5
Temperature chart speed (in/min)	.2	.2	.2
$\bar{P}$	.157	.118	.060

Table 27. BET data for 0.1 wt% moly-alumina catalyst.

Weight = 0.2452 gm			
Run	1	2	3
Helium pressure (in H <sub>2</sub> O)	26.	27.7	29.0
Nitrogen pressure (in H <sub>2</sub> O)	6.4	4.4	1.5
Nitrogen flow meter	50.	41.	26.
Attenuation of desorption peak	x64	x64	x64
Area of desorption peak	195.5	182.0	163.7
Attenuation of calibration peak	x4	x4	x4
Volume of calibration gas (cm <sup>3</sup> )	.19	.19	.19
Area of calibration peak	56.1	56.9	56.7
Concentration chart speed (in/min)	.5	.5	.5
Temperature chart speed (in/min)	.2	.2	.2
$\bar{p}$	.148	.110	.059

Table 28. BET data for pure treated silica.

Weight = 0.1232 gm			
Run	1	2	3
Helium pressure (in H <sub>2</sub> O)	26.	27.7	29.2
Nitrogen pressure (in H <sub>2</sub> O)	6.7	4.5	1.3
Nitrogen flow meter	50.5	42.0	26.5
Attenuation of desorption peak	x64	x64	x64
Area of desorption peak	194.	180.	160.8
Attenuation of calibration peak	x4	x4	x4
Volume of calibration gas (cm <sup>3</sup> )	.19	.19	.19
Area of calibration peak	58.	57.	58.1
Concentration chart speed (in/min)	.5	.5	.5
Temperature chart speed (in/min)	.2	.2	.2
$\bar{p}$	.155	.116	.060

Table 29. BET data for 0.1 wt% moly-silica catalyst.

Weight = 0.1033 gm			
Run	1	2	3
Helium pressure (in H <sub>2</sub> O)	26.	27.7	29.2
Nitrogen pressure (in H <sub>2</sub> O)	7.	4.6	1.5
Nitrogen flow meter	51.5	42.	26.
Attenuation of desorption peak	x64	x64	x64
Area of desorption peak	162.5	151.4	133.0, 131.8
Attenuation of calibration peak	x4	x4	x4
Volume of calibration gas (cm <sup>3</sup> )	.19	.19	.19
Area of calibration peak	57.	55.	56.2
Concentration chart speed (in/min)	.5	.5	.5
Temperature chart speed (in/min)	.2	.2	.2
$\bar{P}$	.158	.114	.059



Table 30. BET data for 5 wt% moly-silica catalyst.

Weight = 0.1194 gm			
Run	1	2	3
Helium pressure (in H <sub>2</sub> O)	26.	27.7	29.2
Nitrogen pressure (in H <sub>2</sub> O)	7.	4.5	1.2
Nitrogen flow meter	50.5	40.5	26.
Attenuation of desorption peak	x32	x32	x32
Area of desorption peak	308.3, 307.6	278.9	250.6
Attenuation of calibration peak	x4	x4	x4
Volume of calibration gas (cm <sup>3</sup> )	.19	.19	.19
Area of calibration peak	58.5	57.2	55.4
Concentration chart speed (in/min)	.5	.5	.5
Temperature chart speed (in/min)	.2	.2	.2
$\bar{p}$	.151	.110	.058

Table 31. BET data for 10 wt% moly-alumina catalyst.

Weight = 0.1199 gm			
Run	1	2	3
Helium pressure (in H <sub>2</sub> O)	26.	27.7	29.2
Nitrogen pressure (in H <sub>2</sub> O)	6.5	4.5	1.5
Nitrogen flow meter	51.	42.	25.
Attenuation of desorption peak	x32	x32	x32
Area of desorption peak	266.8, 263.2	245.	213.4
Attenuation of calibration peak	x4	x4	x4
Volume of calibration gas (cm <sup>3</sup> )	.19	.19	.19
Area of calibration peak	57.5	57.1	57.3
Concentration chart speed (in/min)	.5	.5	.5
Temperature chart speed (in/min)	.2	.2	.2
$\bar{p}$	.154	.113	.056

Table 32. BET data for 15 wt% moly-alumina catalyst.

Weight = 0.1173 gm			
Run	1	2	3
Helium pressure (in H <sub>2</sub> O)	26.	27.7	29.2
Nitrogen pressure (in H <sub>2</sub> O)	6.8	4.7	1.7
Nitrogen flow meter	51.	41.	25.5
Attenuation of desorption peak	x32	x32	x32
Area of desorption peak	199.6	186.6	166.1
Attenuation of calibration peak	x4	x4	x4
Volume of calibration gas (cm <sup>3</sup> )	.19	.19	.19
Area of calibration peak	56.5	55.8	56.
Concentration chart speed (in/min)	.5	.5	.5
Temperature chart speed (in/min)	.2	.2	.2
$\bar{P}$	.155	.108	.062

Table 33. BET data for 20 wt% moly-silica catalyst.

Weight = 0.1233 gm			
Run	1	2	3
Helium pressure (in H <sub>2</sub> O)	26.	27.7	29.2
Nitrogen pressure (in H <sub>2</sub> O)	6.8	4.4	1.0
Nitrogen flow meter	52.	41.	24.5
Attenuation of desorption peak	x64	x32	x32
Area of desorption peak	99.4	186.0	163.4
Attenuation of calibration peak	x4	x4	x4
Volume of calibration gas (cm <sup>3</sup> )	.19	.19	.19
Area of calibration peak	57.0	57.7	55.5
Concentration chart speed (in/min)	.5	.5	.5
Temperature chart speed (in/min)	.2	.2	.2
$\bar{p}$	.158	.107	.056

APPENDIX E  
DIFFERENTIAL REACTOR DATA

Composition of the calibration sample = 90%  $C_6H_{12}$ , 10%  $C_6H_6$ .

Injection size =  $10^{-3}$  ml.

Area of the  $C_6H_{12}$  peak = 7997900.

Area of the  $C_6H_6$  peak = 989530.

Table 34. Raw data for cyclohexane dehydrogenation on moly-alumina catalyst.

Sample	Run	Area of Peak				Weight
		N <sub>2</sub>	H <sub>2</sub> O	C <sub>6</sub> H <sub>12</sub>	C <sub>6</sub> H <sub>6</sub>	
0.1 wt%	1	2772100	8283	228700	---	1.0008
	2	2765800	---	225090	---	
	3	2768700	12322	223450	---	
5 wt%	1	2736500	13337	247950	3720	1.0048
	2	2733800	10308	247040	4007	
	3	2726200	10238	245290	4301	
	4	2729900	8095	244130	4698	
10 wt%	1	2695400	24239	231510	12897	1.0121
	2	2677400	16161	222650	18362	
	3	2683200	12767	220640	20040	
	4	2688200	11198	216260	20319	
15 wt%	1	2700400	24510	212250	17069	0.6394
	2	2696300	14926	213440	20762	
	3	2687400	12976	216220	22786	
	4	2701300	9907	214040	22874	
25 wt%	1	2639800	63255	214630	20837	0.6828
	2	2657100	21910	223140	26947	
	3	2662000	16954	223080	28707	
	4	2667600	15420	219990	29479	

Feed flow rate = 10 ml/56.8 sec.

Table 35. Raw data for cyclohexane dehydrogenation on moly-silica catalyst.

Sample	Run	Area of Peak				Weight
		N <sub>2</sub>	H <sub>2</sub> O	C <sub>6</sub> H <sub>12</sub>	C <sub>6</sub> H <sub>6</sub>	
5 wt%	1	2750900	10698	279670	1028	0.6022
	2	2749600	7183	279070	378	
	3	2750100	5955	274340	722	
	4	2742600	---	270570	568	
10 wt%	1	2772200	13018	273580	2968	0.6015
	2	2756900	9118	277090	1760	
	3	2750300	7533	275910	1503	
	4	2750100	7202	269320	1434	
15 wt%	1	2766500	21658	253360	10703	0.6039
	2	2753300	8665	263380	5719	
	3	2748600	6872	257400	4566	
	4	2747000	6297	256490	3316	
20 wt%	1	2694300	123530	223440	13960	0.5960
	2	2750400	12218	237020	8131	
	3	2752700	8944	238760	6063	
	4	2753100	7879	237230	5144	

---

 Feed flow rate = 10 ml/57.94 sec.

APPENDIX F  
ERROR ANALYSIS OF THE PACKING FACTOR  
VALUES

Error contributed by:

1. The thermocouple cold junction =  $\pm 0.2\%$
2. The K-type thermocouple wire =  $\pm 0.4\%$
3. T.C.Detector plus integrator =  $\pm 1.0\%$
4. Temperature recorder =  $\pm 0.5\%$

Total error =  $\pm 2.1\%$



## LIST OF REFERENCES

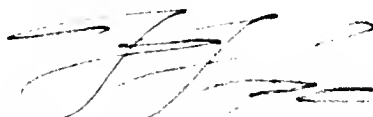
- Adler, S.F., and J.J. Kearney, J. Phys. Chem., 64, 208 (1960).
- Anderson, R., "Experimental Methods in Catalytic Research," Academic Press, New York (1968).
- Bartholomew, C.H., and M. Boudart, J. Catal., 29, 278 (1973).
- Brunauer, S., "The Adsorption of Gases and Vapors--Physical Adsorption," Princeton University, Princeton, NJ (1943).
- Brunauer, S., and P.H. Emmett, J. Am. Chem. Soc., 62, 1732 (1940).
- Brunauer, S., P.H. Emmett, and E. Teller, J. Am. Chem. Soc., 60, 309 (1938).
- Clark, A., "The Theory of Adsorption and Catalysis," Academic Press, New York (1970).
- Emmett, P.H., and S. Brunauer, J. Am. Chem. Soc., 59, 1553 (1937).
- Garcia Fierro, J.L., S. Mendioroz, J.A. Pajares, and S.W. Weller, J. Catal., 65, 263 (1980).
- Herz, R.K., J.B. Kiela, and S.P. Marin, J. Catal., 73, 66 (1982).
- Hill, F.N., and P.W. Selwood, J. Am. Chem. Soc., 71, 2522 (1949).
- Liu, H.C., and S.W. Weller, J. Catal., 66, 65 (1980).
- Liu, H.C., L. Yuan, and S.W. Weller, J. Catal., 61, 282 (1980).
- Maggiore, R., N. Giordano, C. Crisafulli, F. Castilli, L. Solarino, and J.C.J. Bart, J. Catal., 60, 193 (1979).
- Massoth, F.E., J. Catal., 30, 204 (1973).

- Miller, D.J., Ph.D. Dissertation, University of Florida (1982).
- Miller, D.J., and H.H. Lee, *AIChE J.*, 30, 84 (1984).
- Millman, W.S., M. Crespín, A.C. Crillo, Jr., S. Abdo, and W.K. Hall, *J. Catal.*, 60, 404 (1979).
- Parekh, B.S., and S.W. Weller, *J. Catal.*, 47, 100 (1977).
- Parekh, B.S., and S.W. Weller, *J. Catal.*, 55, 58 (1978).
- Phipps, A.M., and D.N. Hume, *J. Chem. Educ.*, 45, 664 (1968).
- Ricca, F., "Adsorption-Desorption Phenomena," Academic Press, New York (1972).
- Ross, S., and J.P. Oliver, "On Physical Adsorption," J.W. Wiley, New York (1964).
- Sarakany, J., and Richard D. Gonzalez, *J. Catal.*, 76, 75 (1982).
- Segawa, K.I., and W.K. Hall, *J. Catal.*, 63, 447 (1983).
- Sinfelt, J., *Chem. Eng. Prog.*, 63, 16 (1967).
- Spenedal, L., and M. Boudart, *J. Phys. Chem.*, 64, 204 (1960).
- Srinivasan, R., H.C. Liu, and S.W. Weller, *J. Catal.*, 57, 87 (1979).
- Stencel, J.M., L.E. Makovsky, and T.A. Sarkus, Submitted to *J. Catal.*, (1983).
- Vaylon, J., and W.K. Hall, *J. Catal.*, 84, 216 (1983).
- Wagner, C.D., W.M. Riggs, L.E. Davis, J.F. Moulder, and G.E. Muilenberg, "Handbook of X-Ray Photoelectron Spectroscopy," Perkin Elmer Corporation, Minnesota (1979).
- Wanke, S.E., B.K. Lotochinski, and H.C. Sidwell, *Can. J. Chem. Eng.*, 59, 357 (1981).
- Weller, W.S., and Sterling E. Voltz, *J. Am. Chem. Soc.*, 76, 4695 (1954).
- Young, D.M., and A.D. Crowell, "Physical Adsorption of Gases," Butterworth, London (1962).

### BIOGRAPHICAL SKETCH

The author was born and raised in Lahore, Pakistan. He earned his B.Sc. degree in chemical engineering from the University of Engineering and Technology, Lahore, Pakistan, in 1979. He came to the United States of America in September 1979 to join the Tennessee Technological University, Cookeville, Tennessee, where he took his masters degree in chemical engineering, graduating in August 1981. In August 1981, he came to Gainesville and has been working on a Ph.D. degree in chemical engineering at the University of Florida. He is interested in conducting applied research in the field of reaction engineering and catalysis.

I certify that I have read this study and that in my opinion it conforms to acceptable standards of scholarly presentation and is fully adequate, in scope and in quality, as a dissertation for the degree of Doctor of Philosophy.



---

Hong H. Lee, Chairman  
Associate Professor of Chemical  
Engineering

I certify that I have read this study and that in my opinion it conforms to acceptable standards of scholarly presentation and is fully adequate, in scope and in quality, as a dissertation for the degree of Doctor of Philosophy.



---

Gar B. Hoflund  
Associate Professor of Chemical  
Engineering

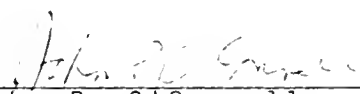
I certify that I have read this study and that in my opinion it conforms to acceptable standards of scholarly presentation and is fully adequate, in scope and in quality, as a dissertation for the degree of Doctor of Philosophy.



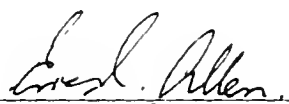
---

Gerald B. Westermann-Clark  
Assistant Professor of Chemical  
Engineering

I certify that I have read this study and that in my opinion it conforms to acceptable standards of scholarly presentation and is fully adequate, in scope and in quality, as a dissertation for the degree of Doctor of Philosophy.

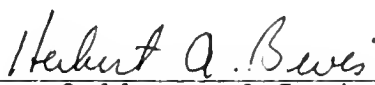
  
\_\_\_\_\_  
John P. O'Connell  
Professor of Chemical Engineering

I certify that I have read this study and that in my opinion it conforms to acceptable standards of scholarly presentation and is fully adequate, in scope and in quality, as a dissertation for the degree of Doctor of Philosophy.

  
\_\_\_\_\_  
Eric R. Allen  
Professor of Environmental  
Engineering Sciences

This dissertation was submitted to the Graduate Faculty of the College of Engineering and to the Graduate School and was accepted as partial fulfillment of the requirements for the degree of Doctor of Philosophy.

May, 1985

  
\_\_\_\_\_  
Dean, College of Engineering

\_\_\_\_\_  
Dean, Graduate School

